Biomass and Bioenergy 203 (2025) 108321

Contents lists available at ScienceDirect

Biomass and Bioenergy

journal homepage: www.elsevier.com/locate/biombioe

Prediction of polycyclic aromatic hydrocarbon species formation using chemical reaction engineering and chemical kinetics models: Effects of pyrolysis parameters and biomass composition

Teka Tesfaye Mengesha [a,b,*], Venkata Ramayya Ancha [b], Alberto Cuoci [c], Bruno Glaser [d], Annett Pollex [e]

[a] Oromia Agricultural Research Institute, Jimma Agricultural Engineering Research Center, Renewable Energy Engineering, Jimma, Ethiopia
[b] Jimma University, Jimma Institute of Technology, Faculty of Mechanical Engineering, P.O.Box 378, Jimma, Ethiopia
[c] CRECK Modeling Lab, Department of Chemistry, Materials, and Chemical Engineering "G. Natta", Politecnico di Milano, P.zza Leonardo da Vinci 32, 20133, Milano, Italy
[d] Soil Biogeochemistry, Martin Luther University Halle-Wittenberg, Halle (Saale), Germany
[e] DBFZ Deutsches Biomasse Forschungszentrum gemeinnützige GmbH, Torgauer Straße 116, D-04347, Leipzig, Germany

ARTICLE INFO

Keywords:
Biomass
Pyrolysis
Polycyclic aromatic hydrocarbons (PAHs)
Biochar
Kinetic modeling

ABSTRACT

Biochar, a valuable byproduct of biomass pyrolysis, offers significant potential for various applications, but the formation of toxic polycyclic aromatic hydrocarbons (PAHs) during its production remains a critical concern. This study introduces a novel approach by employing the Chemical Reaction Engineering and Chemical Kinetics (CRECK) model to predict the fraction of specific PAH species formed at the core stage of slow pyrolysis. This contrasts with prior studies that focused on species data measurements taken at the reactor outlet from reaction product exit routes under high-temperature (840–1800 K) for either gasification or combustion conditions but not for slow pyrolysis. The CRECK Solid Biomass (CRECK-S-B) model was applied to coffee husk and corncob biomass at heating rates of 2, 10, 20, and 30 °C min^{-1} and temperatures ranging from 350 to 750 °C. The model's predictions, which generate tar species varying in composition and quantity depending on the heating rate, were used as input for the OpenSmoke gas-phase batch reactor model, with results validated against experimental data. Key findings reveal that the 450–550 °C range favors PAH formation, with the maximum naphthalene ($C_{10}H_8$) fraction (0.0011) occurring at 450 °C, 3000 s, and 10 °C min^{-1}, strongly influenced by naphthyl ($C_{10}H_7$) concentration. To minimize PAH content in biochar, we recommend maintaining temperatures above 500 °C, using a low heating rate (2 °C min^{-1}), and extending biomass residence times beyond 50 min. This study underscores the need for comprehensive experimental studies to further investigate the combined effects of pyrolysis parameters on PAH formation and to optimize biochar production.

1. Introduction

Biomass pyrolysis is increasingly recognized as a promising method for producing biochar, a carbon-rich solid material generated through the thermochemical conversion of biomass in an oxygen-limited environment. Biochar holds potential for various applications, including agriculture, environmental remediation, and material development, such as biodegradable mulch films, where its incorporation into composites enhances thermal and mechanical properties [1,2]. However, the pyrolysis process, while producing valuable biochar, also generates PAHs, a class of organic compounds consisting of two or more fused aromatic rings. Many PAHs are known or suspected of carcinogens, mutagens, and endocrine disruptors, posing potential risks to human health and the environment. Despite the agricultural benefits of biochar, the presence of PAH and their derivatives on the biochar surfaces poses significant environmental risks. However, the certification of biochar according to standards such as the World Biochar Certificate [3,4] can mitigate these risks by ensuring that the biochar meets certain quality

* Corresponding author. Oromia Agricultural Research Institute, Jimma Agricultural Engineering Research Center, Renewable Energy Engineering, Jimma, Ethiopia.
E-mail addresses: teka.tesfaye@ju.edu.et, tekamen@yahoo.com (T.T. Mengesha), dra.venkata@ju.edu.et (V.R. Ancha), alberto.cuoci@polimi.it (A. Cuoci), bruno.glaser@gmx.de (B. Glaser), Annett.Pollex@dbfz.de (A. Pollex).

https://doi.org/10.1016/j.biombioe.2025.108321
Received 1 February 2025; Received in revised form 22 July 2025; Accepted 24 August 2025
Available online 28 August 2025

and safety criteria. The Certification programs encourage research and development in biochar production techniques that minimize the formation of PAHs leading to the development of cleaner production methods that further reduce environmental risks.

These toxic compounds can originate from contaminated feedstock or form during the pyrolysis process. Soil, surface water, and groundwater are particularly vulnerable to PAH contamination, given their carcinogenic, teratogenic, and mutagenic properties [5]. The United States Environmental Protection Agency (USEPA) released a list of 16 PAHs, which are generally accepted as representatives for all PAHs: naphthalene ($C_{10}H_8$), acenaphthylene ($C_{12}H_8$), acenaphthene ($C_{12}H_{10}$), fluorene ($C_{13}H_{10}$), phenanthrene ($C_{14}H_{10}$), anthracene ($C_{14}H_{10}$), fluoranthene ($C_{16}H_{10}$), pyrene ($C_{16}H_{10}$), benzo[a]anthracene ($C_{18}H_{12}$), chrysene ($C_{18}H_{12}$), benzo[b]fluoranthene ($C_{20}H_{12}$), benzo[k]fluoranthene ($C_{20}H_{12}$), benzo[a]pyrene ($C_{20}H_{12}$), dibenz[a,h]anthracene ($C_{22}H_{14}$), benzo[g,h, i]perylene ($C_{22}H_{12}$), indeno[1,2,3,c,d]pyrene ($C_{22}H_{12}$) [6,7]. Thus, controlling the formation of PAHs is a significant concern in thermal processes [8].

The formation of PAHs during pyrolysis is a complex process governed by several interconnected factors. The effects of pyrolysis parameters, such as residence time, temperature, and heating rate, are crucial in determining the quality of the resulting biochar [9,10]. Simultaneously, the feedstock's intrinsic properties, including its chemical composition (e.g., lignin, cellulose, and hemicellulose content) and structural differences, significantly influence the formation and distribution of PAHs by determining the availability of aromatic precursors [11]. Despite extensive research, the production and valorization of biochar with requisite attributes remain challenging due to the complex nature of biomass. Accurately predicting the amount and composition of PAHs is critical, yet difficult. While conventional experimental studies provide valuable data on the effects of pyrolysis parameters and feedstock composition [12], their time-consuming and resource-intensive nature necessitates the exploration of alternative predictive approaches like kinetic modeling [13]. However, a significant hurdle persists: although numerous biomass mechanisms are documented, most treat biomass holistically, with detailed mechanisms for individual components being sparse and often incomplete [14]. To effectively optimize the pyrolysis process and minimize PAH fractions in biochar, it is essential to model the relationships between feedstock type and pyrolysis parameters. Since the final PAH concentration is critically determined by the biomass composition and reactor design, optimizing these variables is key [15]. This approach ensures the production of biochar that meets quality standards with minimal PAH content and reduced environmental risk, underscoring the importance of precise control over reactor design and operation.

Kinetic modeling is essential for predicting reaction pathways and product distributions during biomass pyrolysis, aiding in reactor design and process optimization [16]. The CRECK Modeling Group at Politecnico di Milano has developed a comprehensive kinetic mechanism for biomass conversion, which includes devolatilization and gas-phase thermochemical processes. The model incorporates a detailed kinetic mechanism, enabling the prediction of individual PAH species rather than just total PAH content, and hence can be applied to a wide range of feedstocks and pyrolysis conditions, providing a more comprehensive predictive tool. So, the model is applicable across various reactor conditions, offering broad utility for researchers [17]. Thus, the advancement of detailed kinetic models describing the pyrolysis and combustion kinetics, typically validated against a large number of experimental data significantly advances the fundamental understanding of the role of PAHs as soot precursors [18,19]. The CRECK model's utility and predictive strength are demonstrated through its application by various researchers. For instance, when benzaldehyde oxidation was investigated using a jet-stirred reactor, simulation results obtained from the CRECK kinetic model were reported to provide a better description of benzaldehyde oxidation by predicting mole fraction profiles for key species such as CO, CO_2, phenol, benzene, and cresol [20]. This ability to model complex reaction networks is crucial for explaining phenomena observed under diverse experimental conditions. For example, at a nominal post-shock pressure of 20 bar over a temperature range of 1030–1800 K where the participation of benzyne in the generation of PAH species like indene, naphthalene, acenaphthylene, and all $C_{14}H_{10}$ PAH isomers were reported, which can further lead to the generation of several larger PAHs [21]. Furthermore, the comprehensiveness of such a model is highlighted by its capacity to incorporate multiple formation pathways, including the creation of PAH (indene, naphthalene, and phenanthrene) and mono-aromatic hydrocarbons (benzene and styrene) from the cyclopentadienyl radical [22,23].

Attempts to predict formation of PAHs in detail during biomass pyrolysis appear very limited in open literature. However previous researchers have made some attempts to predict the development of various classes of tar compounds, which are precursors to PAHs, even though during biomass gasification [24,25]. Those studies highlighted the importance of understanding the effects of feedstock particle size and reactor temperature on the devolatilization of biomass [24]. Additionally, trends in the formation of benzene, indene, naphthalene, phenanthrene, and pyrene during the combustion of toluene-based reference fuels in the temperatures range 840–1350 K were reported, with measurements taken at the reactor outlet [25]. In a study investigating PAH and soot formation in a laminar premixed ethylene flame, the focus shifted from core formation to the post-flame region, specifically examining the impact of inlet velocity and the distance between the burner and the stagnation plate on the transition from gas-phase species to soot particles [26,27]. Theoretical and kinetic investigations have also been conducted on the radical behavior of large PAH in soot formation and oxidation within combustion environments rather than pyrolysis condition [28]. Moreover, the effects of n-butanol blends on the formation of PAH species (C_6H_6, C_6H_5OH, C_7H_6O, C_7H_8, C_8H_{10}, C_8H_8, and $C_{10}H_8$) were explored using gas chromatography-mass spectrometry (GC-MS) and the CRECK mechanism in a fuel-rich heptane combustion process within a micro flow reactor, maintaining a controlled wall temperature of 1100 K along the reactor's inner surface [29].

Almost all the previous study targeting prediction of PAH exclusively employed CRECK. And primarily they focused on PAH formation during biomass gasification, fuel combustion, and soot formation, typically under high-temperature conditions and measured in the post-flame region [8]. In this context, previous researchers have predominantly utilized temperatures ranging from 840 to 1800 K, which are closer to gasification conditions rather than the lower temperatures required for slow pyrolysis of biomass for biochar-focused. This research gap is significant, as the effects of lower temperatures, low heating rates, and extended feedstock residence times on PAH formation remain largely unexplored. To reduce PAH emissions at the source, it is essential to understand the formation mechanisms of PAHs during biomass pyrolysis and to investigate their regulatory mechanisms [30].

In contrast, this study investigates the influence of residence time, heating rate, temperature, and feedstock composition on PAH formation during the slow pyrolysis of corn cob and coffee husk. By coupling the CRECK-S-B biomass pyrolysis model with the OpenSmoke gas-phase batch reactor model, and generating dew point temperature curves for PAH species using Honeywell UniSim design software, this research offers a novel approach to understanding PAH formation under slow pyrolysis conditions. The uniqueness of this work lies in its simulation-based methodology, which predicts the total PAH formation at the core stage of slow pyrolysis. This includes all PAHs produced, regardless of whether they subsequently leave the reactor (in the vapor phase) or become adsorbed onto the biochar, a focus distinct from gasification or combustion conditions. This approach offers a novel perspective, differing from studies that primarily focus on species data collected at various points along the route through which the reaction products, gases, or other substances exit the reactor after the reaction has taken place. By providing insights into the initial stages of PAH formation, this

study advances our understanding of how pyrolysis parameters influence the production of these hazardous compounds. Specifically, the mass fractions of USEPA-listed PAH species were predicted using detailed kinetic mechanisms, followed by validation employing comparable experimental data available to a limited extent, offering valuable guidance for optimizing biochar production to minimize environmental risks.

2. Methods

2.1. Feedstock characterization and determination of the chemical compositions

The study considered coffee husk and corn cob biomass which have varying compositions, resulting in different proportions of volatiles and fixed carbons, which affect their yields. Proximate analysis, moisture content, volatile matter (VM), ash content, and Fixed carbon (FC) (ASTM D3172-13) were performed using a Laboratory unit in the Geological Institute of Ethiopia [31,32].

The elemental composition analysis of coffee husk and corn cob, encompassing carbon (C), hydrogen (H), nitrogen (N), and sulfur (S), was carried out following the DIN EN ISO 16948 standard protocol. The detailed analysis took place at the DBFZ German Biomass Research Center in Germany, with specific results outlined in Table 1. Following the determination of C, H, N, and S content, the oxygen content was subsequently calculated by the principle of difference [33].

Based on the elemental analysis, the biomass characterization method estimates a biochemical composition in terms of the seven reference components; cellulose(CELL), hemicellulose(HCE), lignin-c (LIGC), lignin-h (LIGH), lignin-o(LIGO), tannins(TANN) and triglycerides(TGL) using extended biomass characterization method [34]. The predicted biomass composition must satisfy only the three H, C, and O balances, therefore the ratio that defines three standard mixtures of the main reference species (RM-1, RM-2, and RM-3) which is called splitting parameters was used. These parameters are the degree of freedom of the characterization procedure, which allows one to reduce the five reference species (CELL, HCE, LIGC, LIGH and LIGO) into three mixtures. Any feedstock falling within the triangle bounded by the reference mixture is then considered as a linear combination of those three reference mixtures, to align with the given H/C/O elemental composition [35].

2.2. Biomass devolatilization model for tar species prediction

The CRECK-S-B lumped and multistep kinetic mechanism, comprising 32 reactions and 29 solid species, was employed for thermogravimetric analysis (TGA) to predict tar species formation during biomass devolatilization [38,39]. The chemical composition of the feedstock, including:

CELL, HCE, LIGH, LIGO, TANN, TGL, MOISTURE (for H_2O) and ASH, was used as solid input for the CRECK-S-B TGA model. The model was applied at temperatures of 350, 450, 500, 550, 650, and 750 °C with heating rates of 2, 10, 20, and 30 °C min^{-1}. The tar species listed in Table 3 were predicted for their product fractions, and their sum was compared with experimental results presented in Table 4. The predictions from the biomass devolatilization model, which generate tar species varying in composition and quantity based on the heating rate, were coupled as input to the gas-phase batch reactor model at the same temperatures. These outputs provide the initial conditions for a separate gas-phase kinetic mechanism that models PAH formation. Therefore, although the gas-phase reactions are decoupled from biomass decomposition, the variations in tar composition due to different heating rates ultimately impact the subsequent gas-phase chemistry.

Additionally, any alteration in conditions—such as pressure, and other relevant factors—from one stage to another has been duly taken into account throughout the modeling process.

Table 1
Result of feedstock Characterization.

Proximate analysis, %			Ultimate analysis, %		
	Coffee husk	Corn cob		Coffee husk	Corn cob
Volatile matter	69.11	75.23	C	48.7	46.7
Fixed Carbon	14.99	13.73	H	5.64	5.76
Ash	6.4	3.04	N	1.68	0.46
Moisture	9.5	7.99	O	43.98	47.08
			S	0.16	0.03

Table 2
Splitting parameter and Reference mixture representative for biomass composition prediction [36,37].

Splitting parameter	Molar ratio	A representative for Reference mixture
α	molar ratio of cellulose and hemicellulose	RM-1
β	molar ratio of lignin LIG-O and lignin LIG-C	RM-2
γ	molar ratio of lignin LIG-H and lignin LIG-C	RM-3
δ	molar ratio of lignins (LIG-H and LIG-C) and extractive TGL	RM-2
ε	molar ratio of lignins (LIG-O and LIG-C) and extractive TANN	RM-3

2.3. Batch reactor model for PAH species fraction prediction

The tar species detailed in Table 3, derived from the CRECK-S-B biomass devolatilization model, served as input for the gas-phase batch reactor model across a list of temperatures (350 °C, 450 °C, 500 °C, 550 °C, 650 °C, and 750 °C). For Case 1, the heating time during biomass devolatilization was considered as the residence time, assuming the system is coupled, based on the initial heating rate. The word residence time used here invariably includes heating time. For Case 2, the same residence times (6, 60, 300, 3000, and 6000 s) were used. The gas phase both low and high-temperature kinetic mechanisms (623 species and ~27831 reactions) which include PAH formation up to C_{18} were used. The study focus on the early stages of PAH growth, where individual species are explicitly tracked and not lumped into pseudo-species. The equivalence ratio managed to be zero for which the initial and final mass fractions of nitrogen were equal (inert). Polycyclic aromatic hydrocarbon species fraction was predicted and validated with others experimental results.

2.4. PAH species prediction validation with others experimental data

In this study, validation with other experimental data was systematically conducted to ensure the accuracy and reliability of the results obtained. In the context of predictive modeling, external validation serves as a critical benchmark for evaluating the model's performance in real-world applications. By validating the model with external data, the researcher can verify its predictive accuracy, identify potential biases or overfitting issues, and enhance the model's reliability. This technique plays a vital role in promoting transparency, rigor, and reproducibility in research practices, ultimately contributing to the advancement of knowledge and the development of reliable predictive models in various scientific disciplines. Comparable experimental data available from earlier works [43] were utilized to validate the model's findings regarding the impact of pyrolysis process parameters on the production of PAH species. A comparison was undertaken between the fractions of PAH species predicted by the CRECK model and those obtained from other experimental measurements [44,45] to discern similarities in trends and the relative quantities of these fractions.

Table 3
The tar species considered ([38,40–42]).

Item	Name	Chemical Formula	Description	International Chemical Identifier (InChl)
1	C_2H_3CHO	C_3H_4O	Acrolein	InChI = 1S/C3H4O/c1-2-3-4/h2-3H,1H2
2	C_2H_5CHO	C_3H_6O	Propionaldehyde	InChI = 1S/C3H6O/c1-2-3-4/h3H,2H2,1H3
3	C_2H_5OH	C_2H_6O	Ethanol	InChI = 1S/C2H6O/c1-2-3/h3H,2H2,1H3
4	$C_5H_8O_4$	$C_5H_8O_4$	Xylofuranose	InChI = 1S/C5H8O4/c6-3-2-1-8-5(9-2)4(3)7/h2-7H,1H2/t2-,3+,4-,5-/m1/s1
5	$C_6H_{10}O_5$	$C_6H_{10}O_5$	Levoglucosan	InChI = 1S/C6H10O5/c7-3-2-1-10-6(11-2)5(9)4(3)8/h2-9H,1H2/t2-,3+,4-,5-,6+/m1/s1
6	$C_6H_5OCH_3$	C_7H_8O	Anisole	InChI = 1S/C7H8O/c1-8-7-5-3-2-4-6-7/h2-6H,1H3
7	C_6H_5OH	C_6H_6O	Phenol	InChI = 1S/C6H6O/c7-6-4-2-1-3-5-6/h1-5,7H
8	$C_6H_6O_3$	$C_6H_6O_3$	Hydroxymethyl-furfural	InChI = 1S/C6H6O3/c7-3-5-1-2-6(4–8)9-5/h1-3,8H,4H2
9	$C_{24}H_{28}O_4$	$C_{24}H_{28}O_4$	Heavy Molecular Weight Lignin	InChI = 1S/C24H28O4/c1-5-21(17-9-13-19(14-10-17)27-23(25)7-3)22(6-2)18-11-15-20(16-12-18)28-24(26)8-4/h9-16H,5–8H2,1–4H3/b22-21+
10	CH_2OHCH_2CHO	$C_3H_6O_2$	Propionic Acid	InChI = 1S/C3H6O2/c1-2-3(4)5/h2H2,1H3, (H,4,5)
11	CH_2OHCHO	$C_2H_4O_2$	Hydroxy acetaldehyde	InChI = 1S/C2H4O2/c3-1-2-4/h1,4H,2H2
12	CH_3CHO	C_2H_4O	Acetaldehyde	InChI = 1S/C2H4O/c1-2-3/h2H,1H3
13	CH_3CO_2H	$C_2H_4O_2$	Acetic Acid	InChI = 1S/C2H4O2/c1-2(3)4/h1H3, (H,3,4)
14	CH_3OH	CH_4O	Methanol	InChI = 1S/CH4O/c1-2/h2H,1H3
15	CHOCHO	$C_2H_2O_2$	Glyoxal	InChI = 1S/C2H2O2/c3-1-2-4/h1-2H
16	CRESOL/ $CH_3C_6H_4(OH)$	C_7H_8O	Cresol	InChI = 1S/C7H8O/c1-6-4-2-3-5-7(6)8/h2-5,8H,1H3
17	FURFURAL/ C_4H_3OCHO	$C_5H_4O_2$	2-Furaldehyde	InChI = 1S/C5H4O2/c6-4-5-2-1-3-7-5/h1-4H
18	H_2O	H_2O	Water from Reactions	InChI = 1S/H2O/h1H2
19	HCOOH	CH_2O_2	Formic Acid	InChI = 1S/CH2O2/c2-1-3/h1H, (H,2,3)
20	MLINO	$C_{19}H_{34}O_2$	Methyl Linoleate	InChI = 1S/C19H34O2/c1-3-4-5-6-7-8-9-10-11-12-13-14-15-16-17-18-19(20)21-2/h7-8,10–11H,3–6,9,12–18H2,1–2H3/b8-7-,11-10+
21	U2ME12	$C_{13}H_{22}O_2$	Linalyl Propionate	InChI = 1S/C13H22O2/c1-6-12(14)15-13(5,7-2)10-8-9-11(3)4/h7,9H,2,6,8,10H2,1,3–5H3
22	VANILLIN	$C_8H_8O_3$	Vanillin	InChI = 1S/C8H8O3/c1-11-8-4-6(5–9)2-3-7(8)10/h2-5,10H,1H3

Table 4
The total tar yield data from experimental work were collected by passing the gas mixture through condensers ([46,47]).

Temperature (°C)	Total yield of tar (wt%)	
	Eucalyptus biomass 10 °C min^{-1}	Bagasse biomass 50 °C min^{-1}
350	44.99	51.32
400	45.48	60.66
450	49.54	65.47
500	50.02	66.13
550	50.19	60.63
600	49.86	59.52

The deviation between the experimental value and the model prediction were determined to calculate accuracy. Accuracy reflects how closely the model prediction aligns with the actual value assumed from other works at various temperatures, [46–48].

$$Deviation = \left(1 - \frac{Experimental\ value}{predicted\ value}\right) * 100$$

Apart from direct comparison, prediction was made for experimental data in Table 5, sourced from open literature [49,50] to validate the model.

The biochar was produced from softwood pellets with a measured moisture content of 10.6 %. The pyrolysis process was conducted in a lab-scale batch reactor equipped with a vertical quartz tube (inner diameter: 50 mm, sample bed depth: ~200 mm), heated externally by a 12 kW infrared gold image furnace (P610C; ULVAC-RIKO, Yokohama, Japan). Key process parameters included pyrolysis temperature, residence time, heating rate, and nitrogen carrier gas flow rate to maintain an inert atmosphere. A condensation system with cold traps was used to collect condensable gases, while non-condensable gases were captured in a gas bag for subsequent analysis. To ensure representative sampling, the biochar was thoroughly mixed, and a subsample (~10 % of the total yield) was ground using a mortar and pestle. From this, a 2 g homogenized subsample was taken, of which ~1 g was used for PAH extraction. The 1 g biochar sample was extracted with 100 mL of toluene via Soxhlet extraction for 36 h. The extract was concentrated to 1 mL under a gentle nitrogen stream and analyzed using GC-MS (Agilent 6890 GC coupled with 5975C MS).

Table 5
Feedstock properties and pyrolysis parameter profiles from the experimental work for PAH measurement, also used for prediction validation.

Characterized softwood pellets				Pyrolysis parameters considered			
Proximate analysis [wt.% (db)]		Ultimate analysis [wt.% (db)]		Temperature (°C)	Residence time (min)	Heating rate (°C min−1)	Carrier gas flow rates (L min−1)
FC	17.2	C	53.7	350	10	5	0
VM	77.2	H	6.7	350	10	5	0.33
Ash	5.7	N	0.0	350	10	5	0.67
		O	33.9	350	40	5	0
				350	40	5	0.33
				350	40	5	0.67
				650	10	5	0
				650	10	5	0.33
				650	10	5	0.67
				650	40	5	0
				650	40	5	0.33
				650	40	5	0.67

Reactor type: lab-scale batch reactor equipped with a vertical quartz tube.

2.5. Rate of production and flux analysis

The rate of production analysis was done for selected PAH species predicted using the gas phase kinetic mechanism done at 450 °C and a heating rate of 10 °C min^{-1} specific condition. Flux analysis, also known as path analysis, was done according to the net reaction fluxes which are a set of sources from the gas phase kinetic mechanism and target species of naphthalene. A dew point temperature curve for PAH species was generated to control the condensation effect during pyrolysis operation using Honeywell Unisim design software.

3. Results and discussion

3.1. Feedstock characterization

Table 6 displays the results of biomass composition prediction utilizing Tables 1 and 2 In proximate analysis, volatile matter signifies the combustible elements in a sample that are emitted as gases when the sample undergoes heating. The volatile matter percentages of 69.11 % and 75.23 % in Table 1 fall within the range of reported volatile matter values [40]. The volatile matter content of biomass impacts the proportions of CELL, HCE, LIGNIN, TANN, and TGL, which significantly influence the composition of pyrolysis products. For instance, Corn cob exhibits a CELL content of 46.59 %, while coffee husk shows 35.13 %. Higher volatile matter content typically leads to increased tar production and reduced char yield, whereas lower volatile matter content results in decreased tar formation and higher char yields [51]. Similarly, the fixed carbon content of biomass affects its composition. Corn cob and coffee husk, for example, have LIGNIN contents of 16.61 % and 30.88 %, respectively. A higher fixed carbon content tends to produce less tar during pyrolysis due to the stability of fixed carbon, a primary component of char that is less prone to breaking down into volatile compounds involved in tar formation [52,53]. As illustrated in Fig. 1, the hydrogen-to-carbon (H/C) and oxygen-to-carbon (O/C) atomic ratio of biomass play vital roles in determining the products generated during pyrolysis, including tar and biochar. Elevated H/C and O/C ratios in biomass typically result in increased tar production during pyrolysis because hydrogen-rich compounds are more likely to form volatile products that can condense into tar. Similarly, oxygen-rich functional groups in biomass can contribute to the formation of volatile compounds that condense into tar. Lower H/C and O/C ratios indicate a higher degree of carbonization and greater biochar stability [54,55].

3.2. Effect of heating rate and temperature on tar species generation during devolatilization

It is evident from Fig. 2 that as temperature increases from 350 °C to 450 °C the predicted tar fraction increases for all the heating rates at varying rates and then stabilizes its content between 450 °C and 650 °C [56]. At a low temperature of 350 °C with a low heating rate of 2 °C min^{-1}, the model produces more tar than at heating rates of 10, 20, and 30 °C min^{-1} because, at the low temperature, the process of decomposition slowly happened due to energy which was given on low. With the increment of temperature, the high concentrations of volatiles at a rapid heating rate favored the formation of volatiles and raised the collision frequency of reactants in the gas phase [57]. The tar fraction was more in the high rate of heating than in the slow rate of heating [58]. As shown in Fig. 2b, the similarity in trends indicates that the model is capturing the fundamental behavior of the system, while the offsets suggest that there are systematic differences between the experimental conditions and the model assumptions.

Table 6
Result of biomass composition prediction.

Splitting parameter		Chemical analysis, mass fraction in %		
			Corn cob	Coffee husk
α	0.6	CELL	46.59	35.13
β	0.8	HCE	25.31	19.08
γ	0.8	LIG-C	2.32	3.99
δ	1	LIG-H	0.00	0.00
ε	1	LIG-O	14.76	25.89
		TANN	0.00	0.00
		TGL	0.00	0.00

3.3. The change in heating rate during devolatilization on PAH species generation

Fig. 3 illustrates the relationship between PAH formation, heating rate, and temperature. At 350 °C (Fig. 3a), lower heating rates (2 °C min^{-1}) result in higher tar yields during devolatilization and consequently a larger mass fraction of PAHs. This is likely because the lower energy input at this temperature is sufficient for devolatilization but minimizes further cracking of the tar products. Conversely, increasing the heating rate reduces the overall conversion efficiency at this low temperature since a high heating rate surpasses the rate at which the feedstock can decompose (constrained by heat transfer limitation with large temperature gradient). When the heating rate exceeds the heat transfer limit for the biomass, it results in partial thermal degradation, which can lead to the formation of undesirable byproducts, including PAHs. While it is true that biomass will ultimately reach the set point temperature given sufficient residence time, the trajectory of temperature increase plays a critical role in determining the nature of the products formed during devolatilization. Specifically, slower heating rates allow for more complete decomposition and minimize the cracking of tar products, which can lead to higher yields of PAHs. Conversely, rapid heating may lead to the formation of PAH precursors due to insufficient time for the biomass to fully decompose at lower temperatures.

At 450 °C (Fig. 3b), the increased temperature promotes tar formation (as seen in Fig. 2b), leading to a higher fraction of PAHs, particularly at a heating rate of 10 °C min^{-1}. However, at higher heating rates (20 and 30 °C min^{-1}), the proportion of low molecular weight PAH species including $C_{18}H_{10}$ slightly decreased whereas the medium molecular weight PAHs like $C_{14}H_{10}$ and $C_{16}H_{10}$ increases to some extent. This suggests that the rapid heating at this temperature favors secondary reactions, potentially converting smaller PAHs into these larger species. But at 500 °C (Fig. 3c), except for the large molecular weight $C_{18}H_{10}$ the fraction of PAH species is increasing with different extent for higher heating rates (10–30 °C min^{-1}).

The formation of heavier PAHs during fast pyrolysis suggests that primary tar compounds undergo secondary gas-phase reactions, as supported by previous research [59]. Fig. 3d, e and 3f demonstrate an increasing trend in PAH species with heating rate but generally, the fraction of PAHs is decreasing with temperature from 550 °C to 750 °C. For these temperatures the rate of increment with heating rate is decreasing. However, the maximum fraction for most PAH species is observed at 450 °C (Fig. 3b), while some others peak at 500 °C. This temperature range (450–550 °C) represents a highly active pyrolysis regime where the influence of heating rate on PAH formation is not direct. This is likely because this temperature range facilitates both the formation of volatile precursors and their subsequent conversion to PAHs through secondary reactions.

3.4. Effect of temperature on PAHs species generation

Temperature is arguably the most critical factor influencing biochar properties during pyrolysis. Biochar yield generally decreases with increasing temperature. As temperature rises, the biochar's carbon content increases. This is because volatile components preferentially convert into gaseous products, leaving behind a more carbonaceous residue. Higher pyrolysis temperatures often lead to increased surface

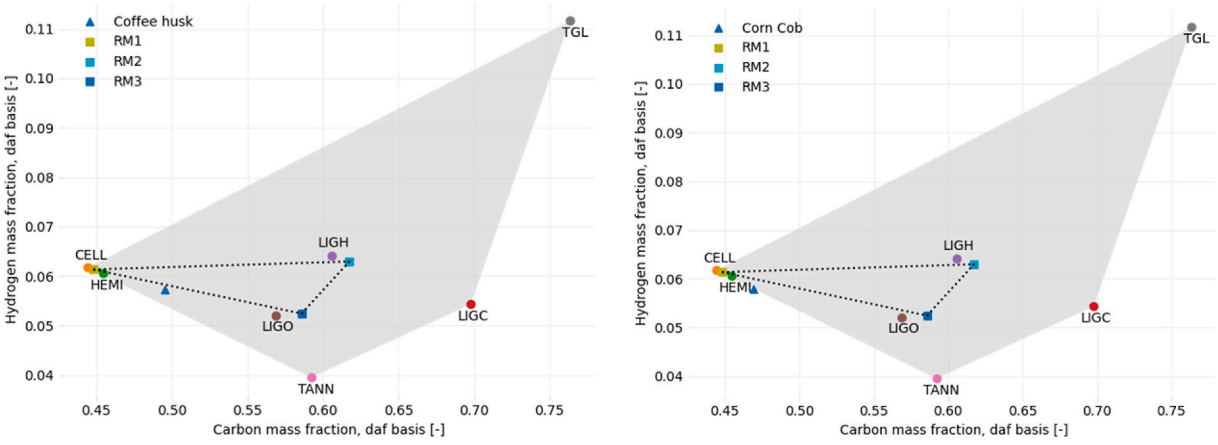

a) Coffee husk b) Corn cob

Fig. 1. Hydrogen vs. Carbon mass fraction plot of biomass samples along with their reference species (https://biocomptool.streamlit.app).

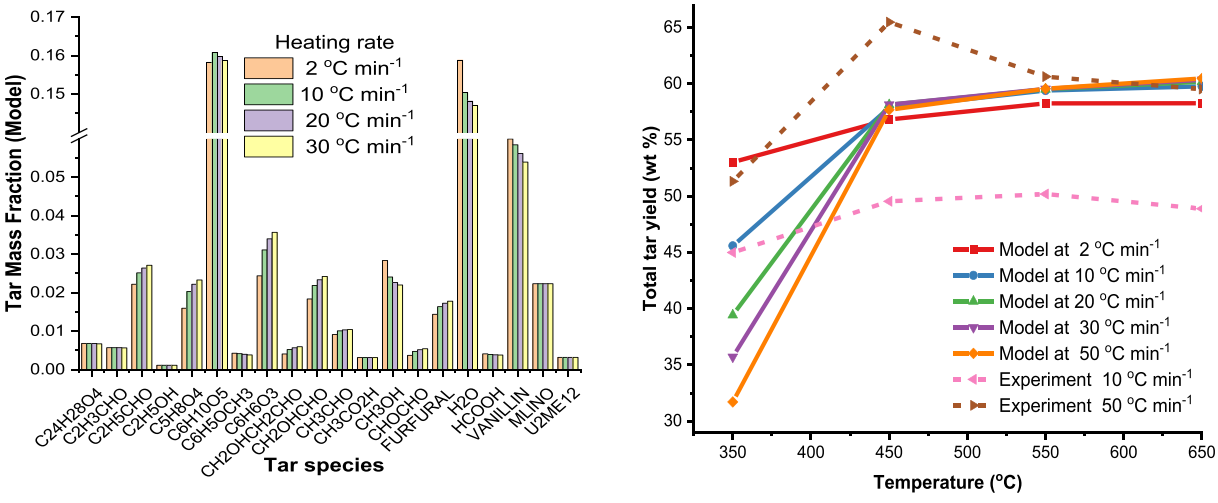

(**a**) Mass fraction at 450 °C (**b**) Model Predictions vs. Experimental Data from Table 4

Fig. 2. The effect of pyrolysis temperature and heating rate on tar (species as listed in (a)) yield during devolatilization.

area and porosity of the biochar. This happens because of micropore formation and organic matter decomposition. These characteristics can enhance the biochar's ability to adsorb pollutants or store nutrients. Temperature can influence the types and amounts of functional groups on the biochar surface. Lower temperatures tend to preserve more oxygen-containing functional groups, which can be beneficial for contaminant adsorption. Higher temperatures might result in the loss of these groups, impacting surface chemistry. Biochar produced at higher temperatures is generally more stable and resistant to degradation in the environment. The optimal temperature for pyrolysis depends on the desired biochar properties and intended application. As a result, temperature plays a crucial role in shaping the characteristics of biochar produced through pyrolysis. Additionally, temperature has a significant influence on the quality and quantity of PAHs in biochar.

Fig. 4a-d illustrates the effect of temperature changes at specific heating rates on the generation of PAH species. At a heating rate of 2 °C min^{-1} except for large molecular weight PAH species, peaks were observed at 350 °C, likely the heating rate allowed sufficient time for thermochemical reactions to equilibrate the temperature between the internal and external surfaces of the biomass [60]. This may be due to the strong intra-chain hydrogen bonds of cellulose functional groups, which increase the likelihood of dehydration reactions at lower temperatures and heating rates [61]. This simultaneous decomposition of the biomass surface and interior reduced the generation of PAH species compared to higher heating rates. However, large ($C_{18}H_{10}$ and $C_{18}H_{14}$) and medium($C_{16}H_{10}$) molecular weight PAH species shifted to 450 °C. According to a study [62], since slower pyrolysis ensures adequate heat conduction, the effectiveness of low-temperature pyrolysis with a heating rate of 5 °C min^{-1} for biochar production was reported. Another experiment [63] done at a 2 °C min^{-1} heating rate demonstrated, a decrease in bio-oil yield as the temperature increased from 450 to 550 °C due to reduced production of condensable vapors—key precursors for PAHs.

As the heating rate increases to 10, 20, and 30 °C min^{-1} as shown in Fig. 4b to d, the peaks shift to 450 and 500 °C, leading to a higher fraction of PAH species. At these higher heating rates, the internal temperature of the biomass struggles to reach the decomposition point, causing delays in thermal cracking due to heat transfer resistance between the heater and samples [64]. Consequently, higher heating rates shift the decomposition curve to higher temperatures, significantly influencing the maximum decomposition rate, which tends to increase and occur at elevated temperatures. Additionally, these rates intensify

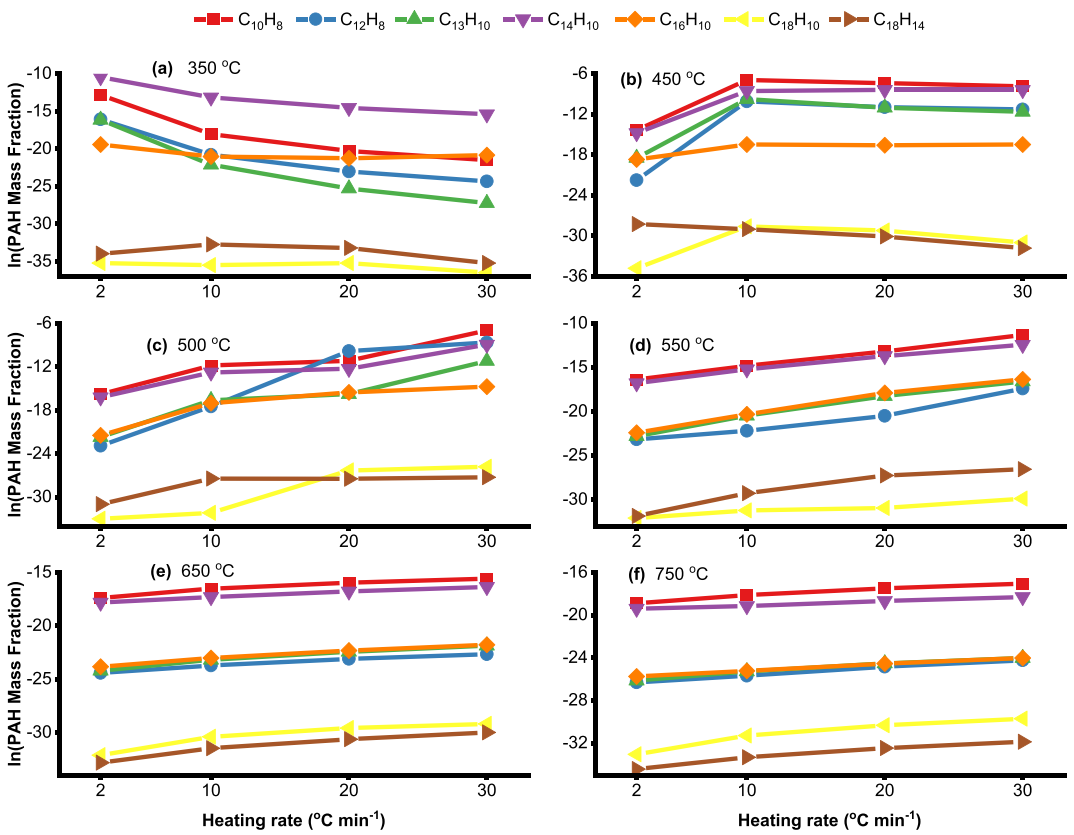

Fig. 3. The heating rate effect at specific temperatures on PAHs species generation converted to Log-scale. The heating time was incorporated into the gas-phase batch reactor model as the residence time, assuming direct coupling of the biomass devolatilization and gas-phase reaction models.

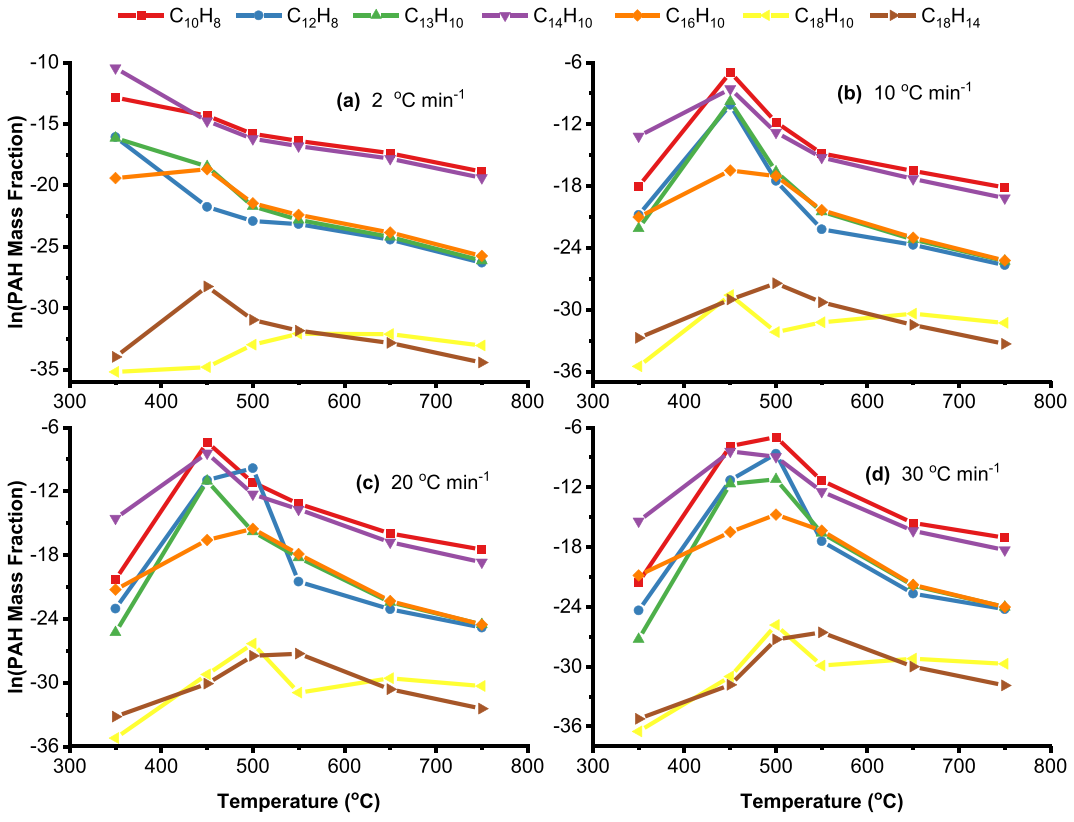

Fig. 4. The effect of temperature at a specific heating rate on PAH species generation converted to Log-scale. The heating time was incorporated into the gas-phase batch reactor model as the residence time, assuming direct coupling of the biomass devolatilization and gas-phase reaction models.

the thermal cracking process due to insufficient interaction among the particles, allowing pyrolysis to continue even at relatively high temperatures.

The findings align with the PAH generation profiles outlined in Ref. [65], where PAH levels peaked at 500 °C before undergoing a rapid decline. But the maximum weight fraction of Fluorene and Naphthalene respectively 5.73E-5 and 9.8E-4 observed at 450 °C and 10 °C min^{-1}. Consistent with [66], increasing the pyrolysis temperature from 450 to 500 °C has led to the formation of medium-molecular-weight PAHs through polymerization. Simultaneously, at a heating rate of 30 °C min^{-1}, complex multiphase and multi-process reactions have resulted in the generation of low-molecular-weight PAHs such as $C_{10}H_8$. Reported similarly by Ref. [67], biochar produced at 350 °C contains fewer 3–4 ring PAHs compared to biochar produced at 450 °C and 500 °C.

Fig. 5a shows the generation of low molecular weight PAHs, such as naphthalene ($C_{10}H_8$), begins at a relatively low temperature (350 °C) with a slow heating rate (2 °C min^{-1}) and generally increases with higher heating rates at other temperatures. The lowest naphthalene fraction (4.53 x 10^{-10}) occurs at 350 °C and 30 °C min^{-1}, likely due to insufficient heat transfer at this combination of low temperature and high heating rate.

At 450 °C and above 10 °C min^{-1}, the naphthalene fraction decreases with increasing heating rate (5.94 x 10^{-7}, 9.8 x 10^{-4}, 6.14 x 10^{-4}, and 3.89 x 10^{-4} at 2, 10, 20, and 30 °C min^{-1}, respectively). However, at 500 °C, the naphthalene fraction increases with the heating rate (1.36 x 10^{-7}, 7.50 x 10^{-6}, 1.42 x 10^{-5}, and 9.44 x 10^{-4} at 2, 10, 20, and 30 °C min^{-1}, respectively) and the trend visualized by the color gradients in Fig. 5a.

Fig. 5b reveals that the maximum pyrene fraction (3.97 x 10^{-7}) is observed at 500 °C and 30 °C min^{-1}, while the minimum (4.45 x 10^{-11}) occurs at 650 °C and 2 °C min^{-1}. Therefore, operating at low heating rates (e.g., 2 °C min^{-1}) and temperatures above 500 °C appear to minimize the formation of PAHs. Similar trends were reported [68] studied at pyrolysis conditions of 450–750 °C temperature and 100 to 400 $^{o}Cmin^{-1}$ heating rate with maximum oil yield obtained at pyrolysis temperature of 500 °C and heating rate of 350 °C min^{-1}. Another study [69] investigated at pyrolysis conditions ranging from 440 to 480 °C temperature and 40–80 °C min^{-1} heating rate and reported the highest bio-oil yield achievement at a pyrolysis temperature of 480 °C and a heating rate of 80 °C min^{-1}.

3.5. Effect of residence time on PAHs species generation

Biomass residence time refers to the duration that solid biomass remains at the peak pyrolysis temperature within the reactor. Prolonged residence times at high temperatures typically result in lower biochar yields, as extended exposure to heat accelerates the decomposition of biomass into volatile products, leaving less solid material for biochar formation. This can also lead to further decomposition and pore collapse, which reduces the surface area. Shorter residence times may preserve more oxygen-containing groups, which are beneficial for contaminant adsorption, whereas longer residence times may lead to the loss of these functional groups. Similarly, gas residence time is the period that the hot gases produced during pyrolysis remain within the reactor. Extended gas residence times can influence the distribution of PAHs within the reactor, affecting their final concentration in the biochar. Therefore, residence time must be carefully managed to avoid excessive heat transfer within the reactor while ensuring the efficient removal of volatile products.

The influence of residence time on PAH species formation is demonstrated in Fig. 6, even when the pyrolysis temperature is held constant. At a heating temperature of 450 °C, the concentration of PAH species significantly increases as the gas residence time extends from a few seconds to several thousand seconds. For instance, the formation of lower molecular weight PAHs like naphthalene ($C_{10}H_8$) peaks at intermediate residence times before declining for longer durations. Whereas higher molecular weight PAH such as pyrene ($C_{16}H_{10}$) reaches its peak under higher temperatures and shorter residence time conditions. The study identifies specific conditions under which the highest concentrations of different PAH species are observed, highlighting the critical role of residence time in determining PAH profiles during pyrolysis. These findings underscore the complex interplay between temperature, heating rate, and residence time in controlling the formation of various PAHs during biomass pyrolysis.

It has been reported that at lower temperatures, a longer gas residence time is necessary, as extended reaction times allow for the completion of thermal decomposition processes, thereby reducing the fraction of PAH species [70]. According to Ref. [71], the concentration of PAHs increases with temperature up to a residence time of 145 s, after which it begins to decline slightly. Short residence times tend to minimize secondary reactions and decrease biochar yield, while longer residence times result in higher biochar yields [72].

As shown in Fig. 6a, Naphthalene's disappearance at long residence

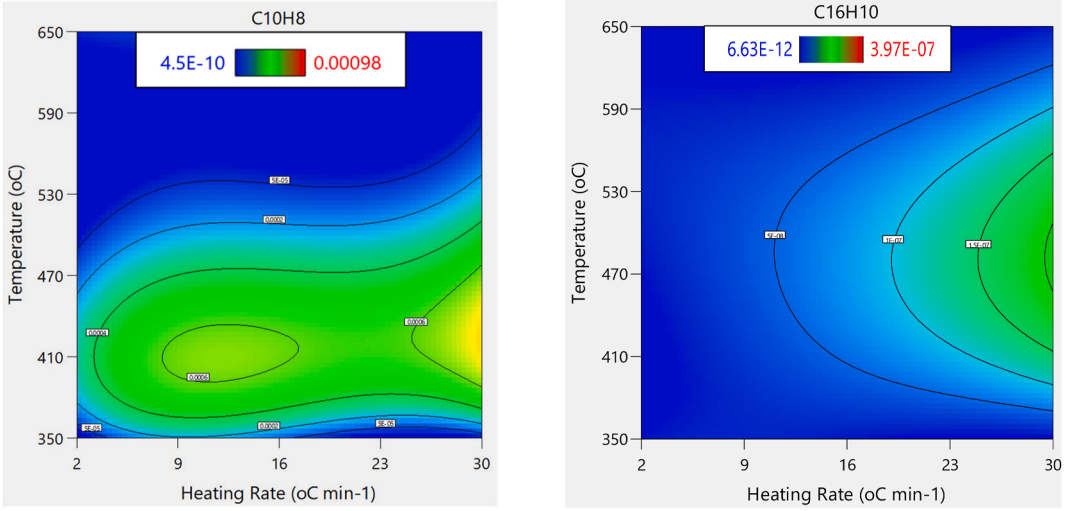

(**a**) Naphthalene ($C_{10}H_8$) (**b**) Pyrene ($C_{16}H_{10}$)

Fig. 5. Effect of temperature and heating rate on PAH species generation using surface graph.

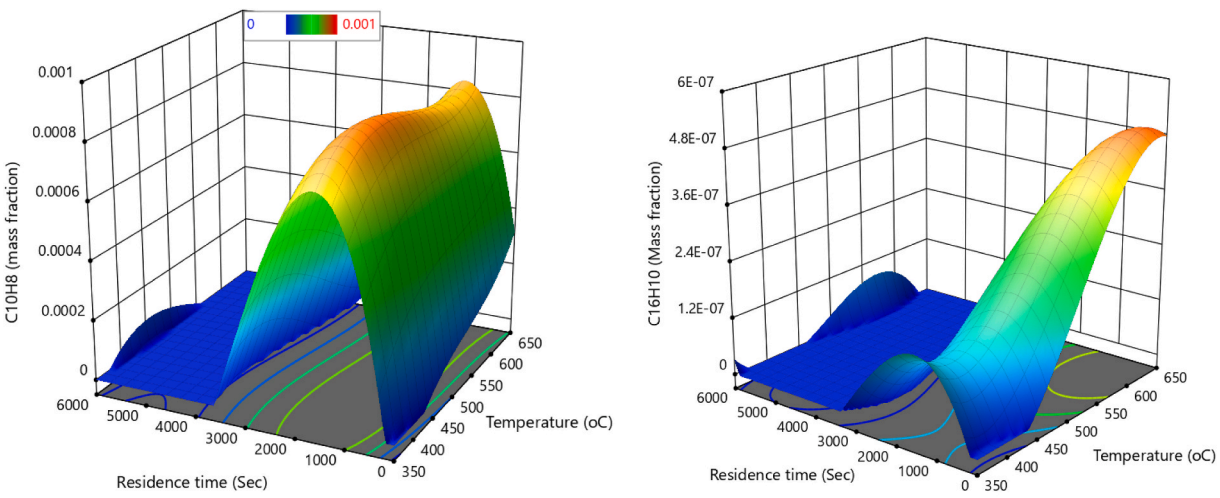

Fig. 6. The effect of residence time at 30 °C min^{-1} heating rate on PAH species generation using 3d surface graph. Residence time (6, 60, 300, 3000, 6000 s) was used.

times is a direct consequence of its role as a key intermediate in a complex reaction network. This network leads to the formation of larger, more stable polycyclic aromatic hydrocarbons (PAHs) and, ultimately, soot. The extended residence time provides the necessary duration for these secondary consumption reactions to proceed toward completion [73,74]. The chemical kinetics model likely incorporates these secondary reaction pathways. At extended residence times, the model demonstrates that the rate of naphthalene consumption—through mechanisms such as thermal cracking, polymerization, and PAH growth reactions—surpasses its rate of formation. This imbalance results in a net decrease in its concentration, eventually reaching zero [75,76]. As residence time increases, secondary reactions become more favorable, consuming the initially formed naphthalene. Thus, it transforms into other products, such as smaller molecules, larger PAHs, or char. This reflects the dynamic nature of PAH formation and transformation in pyrolysis environments, where extended residence times promote extensive secondary chemistry, leading to the depletion of intermediate species like naphthalene. Overall, the impact of residence time is significant in altering the concentration of PAH species during biomass pyrolysis.

3.5.1. Validation result

In both the experimental data and the model, the highest generation of PAH species occurred at 400 °C, except for the medium molecular weight PAH species $C_{16}H_{10}$, which peaked at 500 °C. The deviations observed in Fig. 7a, for naphthalene predictions at 350 °C, 450 °C, 500 °C, and 550 °C are 26.09 %, 34.25 %, 84.37 %, and −42.66 %, respectively. For Acenaphthylene predicted at 350 °C, 450 °C, 500 °C, and 550 °C, the deviations are 3.59 %, 15.89 %, 28.94 %, and 99.46 %, respectively.

Likewise in Fig. 7b, for fluorene predicted at 350 °C, 450 °C, and 550 °C, the deviations are 65.81 %, −2.35 %, and 16.09 %, respectively. Phenanthrene predicted at 350 and 550 °C the deviations observed are 7.43 and 0.097 % respectively. And for fluoranthene predicted at 350, 450, and 550 °C the deviations observed are 93.74, 47.92 and 93.32 % respectively.

As shown in Fig. 8a and b, the model is better at predicting the low molecular weight PAH $C_{10}H_8$. The disparity between the model predictions and experimental values in Fig. 8b may stem from variations in the consideration of pyrolysis process parameters, pyrolysis operation, and the influence of condensation effects. Due to the scarcity of experimental data on PAH formation at the core stage of pyrolysis, the model

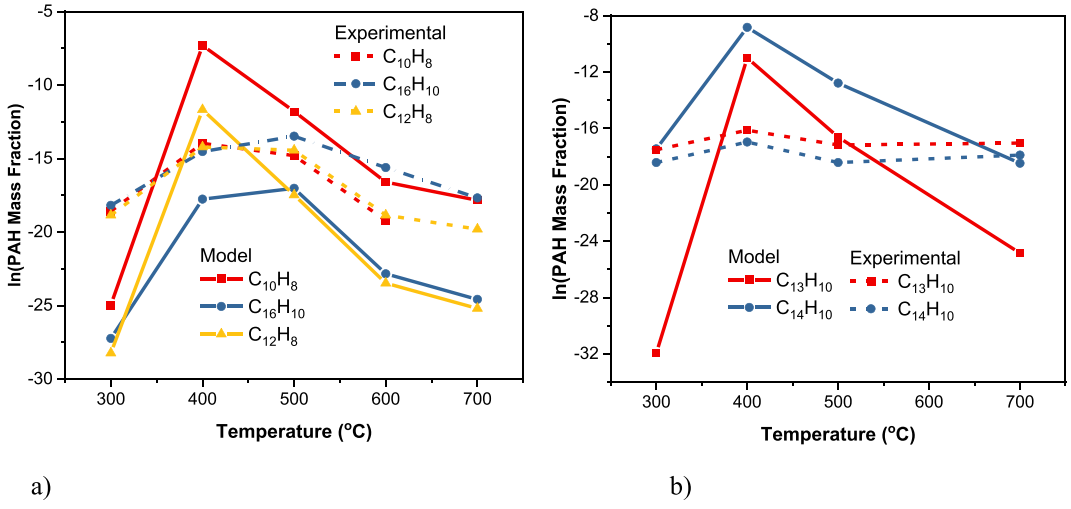

Fig. 7. Graph for Model direct comparison with experimental results, showing the trend of PAHs species generation with temperature converted to Log-scale.

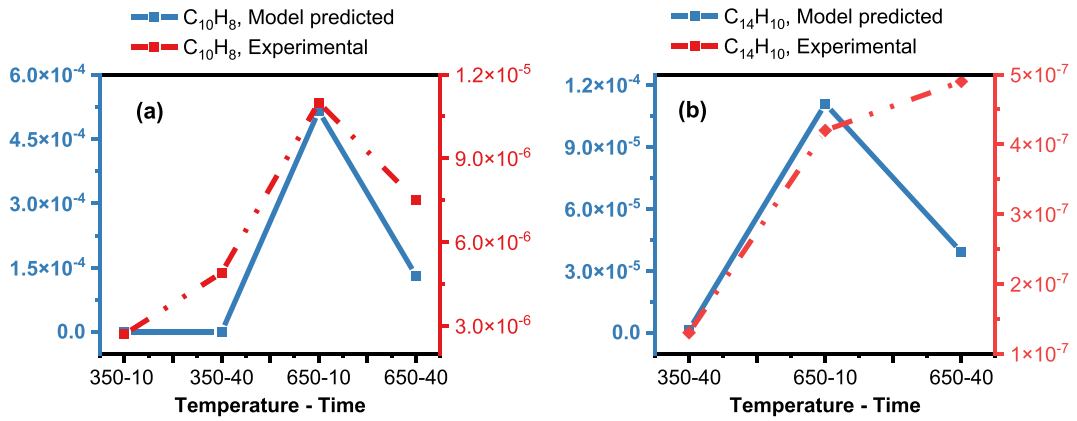

Fig. 8. Graph for depicting Model Validation: Predictions based on experimental data (Table 5) are compared against actual experimental results for verification.

validation relies on reported experimental data for PAHs adsorbed onto the biochar. This approach serves as a first step in assessing the model's performance, as biochar-adsorbed PAH measurements are more commonly available in the literature compared to real-time measurements of PAHs in the pyrolysis vapor stream. Specifically, the experimental data used for validation quantify the PAH content that remains associated with the biochar after pyrolysis, which includes volatile PAH components that have condensed or become trapped on the biochar surface. Almost all the previous study targeting prediction of PAH primarily they focused on PAH formation during biomass gasification, fuel combustion, and soot formation, typically under high-temperature conditions and measured in the post-flame region [8]. The relationship between the release of PAHs in volatiles and the aromatic nature of char during pyrolysis remains unclear. Most studies on PAHs focus solely on influencing factors during combustion and post-combustion emission factors [30].

To grasp PAH partitioning, only a few studies have measured PAH levels in pyrolytic vapors. These investigations usually concentrate solely on temperature effects, directing the gas stream through a cold trap or impinger system to capture the condensable products. The resulting liquid fraction (tar) is then analyzed for PAH concentration, often using a liquid-liquid extraction method [65,77]. Consequently, there is a notable shortage of extensive experimental data that quantifies PAHs across all pyrolysis product streams, which impedes complete model validation. Thus, the combined effects of pyrolysis process parameters on PAH concentrations, as well as the optimal prediction of USEPA-listed PAH species levels, are rarely emphasized [43]. Typically, despite deviations between the model and experimental results, the model effectively highlights the effect of each parameter.

3.6. *Effect of feedstock chemical composition of coffee husk and corn cob*

Lignocellulosic biomass is primarily composed of three components: hemicellulose, cellulose, and lignin. Three different phenylpropane structural units—p-hydroxyphenyl (H), guaiacyl (G), and syringyl (S) units—are joined by carbon-carbon and ether bonds to form the amorphous tridimensional polymer known as lignin. These classes polymerize to create a sophisticated, three-dimensional network that strengthens and stabilizes the cell wall. Lignin's high carbon content makes it a perfect precursor for the production of lignocellulosic biomass-derived biochar when compared to other biomass components [78]. A greater range of temperatures is experienced by lignin during its breakdown, with the production of monolignols at lower temperatures and phenols and light oxygenates at higher temperatures. Other secondary reactions also take place in the solid biomass with increasing temperatures [37] and its decomposition is evident [79] by a gradual decrease in mass. The biochar yield derived from lignin was notably elevated, reaching 45.69 % [80], with the potential to produce approximately 65 % more biochar compared to the pyrolysis of cellulose and hemicellulose as reported [81].

For the thermochemical conversion process, residual biomass feedstock with a high lignin content is highly desirable because it can produce biochar with improved physicochemical characteristics, such as a high fixed carbon content, surface area, and fine aromatic structure, which are necessary for a variety of applications. Since lignin is the primary biochar precursor, it increases the yield of biochar and creates biochar with various physicochemical characteristics during the pyrolysis process. Lignin has a highly aromatic structure, and the thermal degradation pathway is mainly dominated by the free radical reaction pathway. Whereas cellulose at low temperatures undergoes depolymerization followed by several degradation pathways, including intramolecular rearrangement, dehydration, decarboxylation, aromatization, and intermolecular condensation. According to published research [82], cellulose is susceptible to crosslinking reactions following dehydration, which can result in the formation of char. Above 300 °C, cellulose undergoes a markedly enhanced pyrolysis, yielding a greater amount of tar products; at approximately 500 °C, the highest yield of bio-oil is achieved. So, the pyrolysis of cellulose and hemicellulose encourages the production of volatile chemicals.

However, a study [83] investigating the interplay of volatile products from lignin with cellulose revealed that the interaction leads to elevated gaseous products, reduced char, and increased tar yield from both cellulose and lignin. The type of biomass feedstock used for pyrolysis plays a critical role in determining the yield, quality, and PAH content of the resulting biochar. The presence of minerals like potassium (K) or phosphorus (P) in the biomass can result in biochar with a higher nutrient content. This can be beneficial for applications like soil amendment and improving fertility. The chemical composition of the biomass influences the types of functional groups present on the biochar surface. These groups play a role in adsorption capacity, nutrient retention, and overall surface chemistry. Biomass composition is a fundamental factor influencing biochar yield, quality, and PAH formation. Understanding the characteristics of different feedstocks and their behavior during pyrolysis is crucial for selecting suitable materials and optimizing the process to achieve desired biochar properties.

From the study, the difference in the content of cellulose and lignin structure [84] found within the Coffee husk (CH) and Corn Cob (CC) feedstock was observed in Fig. 9.

As reported [85], the relative amounts of lignin's guaiacyl (G) and sinapyl (S) structures and their activity in biomass are key factors in PAH formation. As shown in Table 6, the cellulose fraction is higher in corncob 46.59 % compared to coffee husk 35.13 %, consistent with previous findings [86]. Due to its aromatic structure and propensity to form free radicals during thermal decomposition, biomass with higher lignin content is more likely to generate PAHs during pyrolysis. Consequently, at a low temperature of 350 °C (Fig. 9a), coffee husk generates a

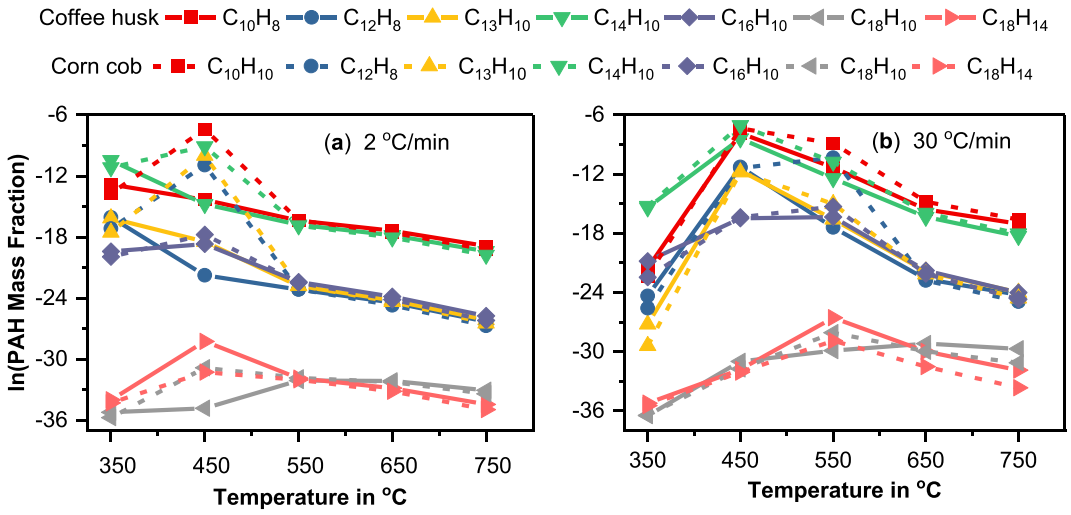

Fig. 9. The effect of Coffee husk and Corn Cob feedstock's constituents on PAH species generation converted to Log-scale.

higher percentage of PAH species than corncob at a heating rate of 2 °C min^{-1}. However, at 450 °C in the same Figure9a except for larger molecular weight PAH species ($C_{18}H_{14}$), corncob produces a higher percentage of PAHs, likely due to the shift to higher temperatures. This is because cellulose, with its simpler structure, is not a direct source of PAHs; rather, its decomposition during pyrolysis generates intermediate compounds that serve as precursors for PAH formation.

The study, using pure cellulose as the feedstock, found that increasing the initial sample mass from 200 mg to 500 mg increased the yield of PAHs [87]. Higher cellulosic biomass feedstock levels promote the formation of free radicals, thereby increasing PAH emission factors [88]. As reported [89], when the depolymerization rate outcompeted the re-polymerization PAHs species generation may decrease. Under a heating rate of 30 °C min^{-1}(Fig. 9b), except $C_{12}H_8$ & $C_{16}H_{10}$ for corn cob and larger molecular weight, the highest PAH species fractions were noted at 450 °C for both feedstocks. The PAH species fraction produced at 2 °Cmin^{-1} and 350 °C is lower compared to that at 30 °C min^{-1} and 450 °C for the coffee husk feedstock, increasing with the heating rate. However, for the corn cob feedstock, it peaks at 2 °C min^{-1} and 450 °C, declining with the heating rate. The increased yield of PAHs can be attributed to the substantially increasing cleavage of methoxyl groups, aliphatic C–C bonds, and carbonyl groups concerning the heating rate for the coffee husk feedstock. Above the temperature of 450 °C reduction of the PAH was reported [90] but the intensity is higher between 350 and 450 °C attributed to the higher lignin content (higher energy bonds). In general, there is a strong correlation between the generation

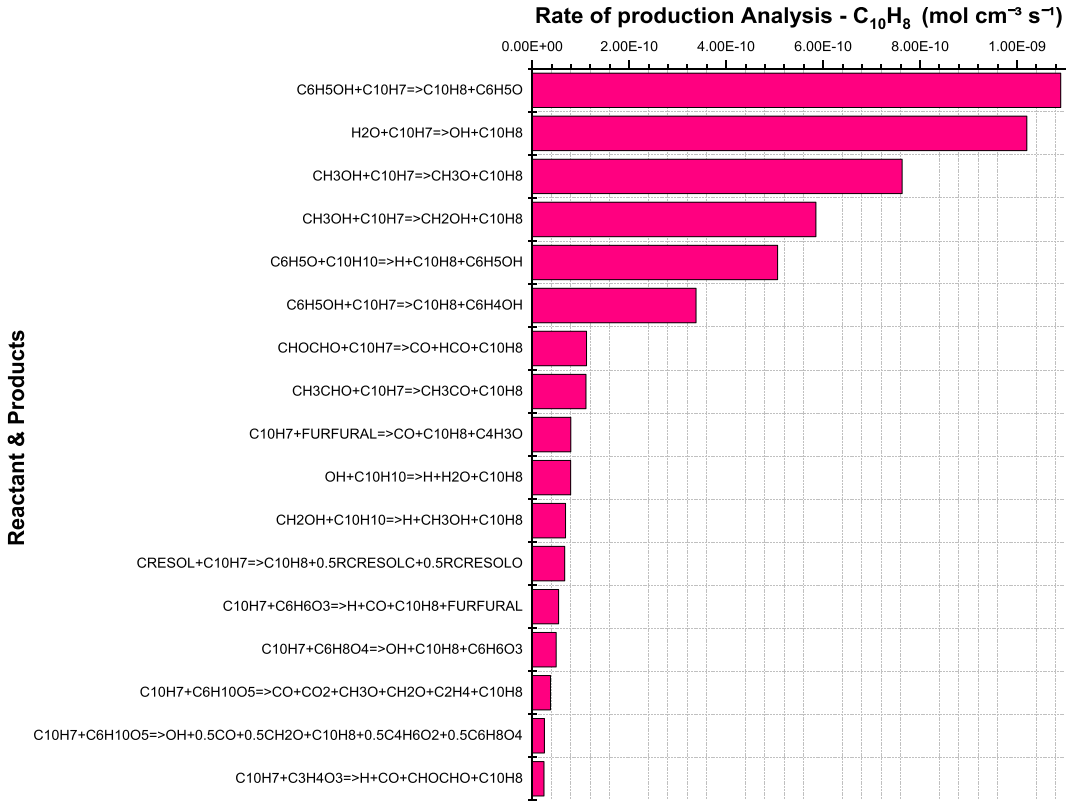

Fig. 10. Rate of production analysis of naphthalene.

of PAHs during pyrolysis and the lignin, cellulose, and hemicellulose content of the feedstock, as indicated by reports [91,92]. Similarly, we can conclude that a feedstock rich in cellulose produces significantly more PAHs than lignin-enriched feedstock at a low heating rate [43,93].

3.7. PAHs species rate of production and reaction path analysis

Understanding the reaction rates and pathways for the formation of specific products, particularly PAHs, is crucial for optimizing processes and mitigating environmental impact. OpenSMOKE++ is a valuable tool for pyrolysis research, as it is a powerful open-source software package designed to model complex reaction systems. It enables the definition of detailed reaction mechanisms involving various PAH precursors, intermediates, and final products. By utilizing kinetic parameters like pre-exponential factors and activation energies, the software can predict reaction rates effectively. Additionally (as shown in Fig. 11), OpenSMOKE++'s functionality for flux analysis enables researchers to pinpoint dominant reaction pathways that lead to specific PAHs. It provides information about the stoichiometry of the reaction and the relative rates of formation or consumption of different reactants and products. This analysis helps to determine the overall reaction rate and the dependencies between different species in the reaction network and also guides rate constant calculations for potential model improvement.

Flux analysis, also known as path analysis, focuses on the flow of reactants and intermediates through different reaction pathways in a reaction network. It evaluates the contributions of different pathways to the overall reaction flux or rate. Flux analysis helps identify the key reaction steps or pathways that dominate the reaction kinetics and influence the distribution of products. This analysis is particularly useful for understanding the reaction mechanism and identifying potential bottlenecks or rate-limiting steps.

Thus, the flux diagram construction process is based on the net reaction fluxes which are a set of sources from the gas phase kinetic mechanism done at 450 °C and heating rate 10 °C min^{-1} and target species of naphthalene. As shown in Fig. 10, the most important naphthalene-forming reactions are $C_6H_5OH + C_{10}H_7$, $H_2O + C_{10}H_7$ and $CH_3OH + C_{10}H_7$. Therefore, these pathways can be classified under functional group transformations or substitution reactions due to the changes in functional groups and substituents that occur during the process of naphthalene formation. So, the rate-of-production (ROP) analysis reveals that $C_{10}H_8$ formation is strongly affected by the naphthyl ($C_{10}H_7$) concentration [94]. The pathway leading to naphthyl radical is important for all the cases studied [21] in terms of percentage contribution to Naphthalene, with the absolute flux depending on the concentrations of naphthyl, phenol (C_6H_5OH) and Methanol (CH_3OH).

According to the report [95], the cyclic pathways involving naphthyl radicals contribute about 70 % to the flux of naphthalene.

The direct connections from RCATEC (0.134 %, likely a catechol

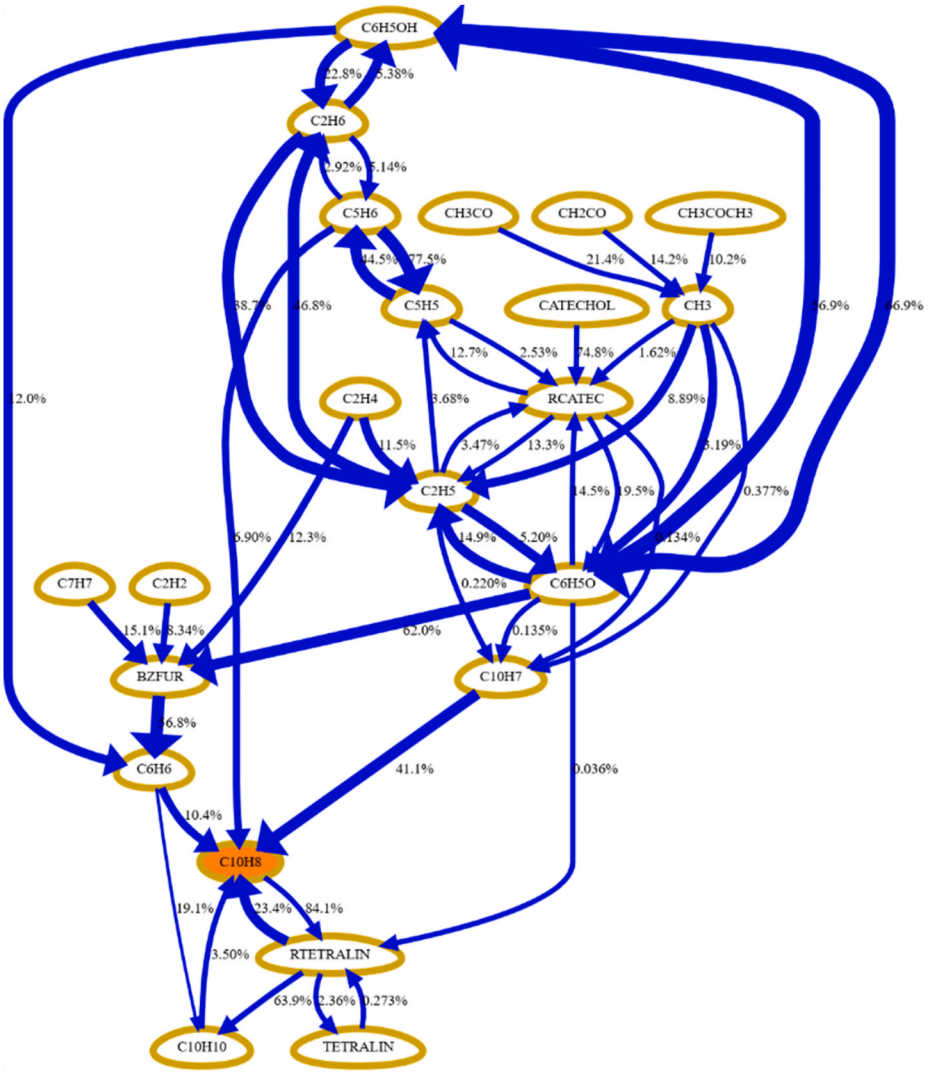

Fig. 11. Naphthalene formation pathways at 450 °C and heating rate 10 °C min^{-1}.

derivative), C_2H_5 (0.22 %, ethyl radical), C_6H_5O (0.135 %, phenoxy radical), and CH_3 (0.377 %, methyl radical) to $C_{10}H_7$ (naphthyl radical) indicate secondary formation pathways, derived from lignin pyrolysis (e.g., LIGCC => $0.7H_2 + 0.7H_2O + 1.15CO + 0.45CH_4 + 0.4C_2H_6 + 0.3C_2H_4 + 0.35CH_2OHCHO + 0.15CRESOL + 0.25VANILLIN + 0.15C_6H_5OCH_3 + 6.8CHAR + 0.4COS$) and radical reactions (e.g., $H + CH_2$ (+M) = CH_3 (+M)). These species recombine or undergo ring expansion/dehydrogenation to form naphthyl, confirming it as a non-primary product from secondary radical processes. The 63.9 % yield from RETRALIN to TETRALIN in Fig. 11 suggests tetralin as a major intermediate, likely from cyclization of aromatic fragments (e.g., $C_6H_5\bullet + C_4H_7\bullet$) via LIGCC, with dehydrogenation to $C_{10}H_7\bullet$ ($C_{10}H_{12} \rightarrow C_{10}H_7 + H_2$) supported by H-abstraction kinetics (e.g., $H + CH_4 = H_2 + CH_3$). This addresses naphthyl's non-primary origin, with precursors contributing 0.866 % directly to $C_{10}H_7$. The figure, by including the connections and the 63.9 % RETRALIN-to-TETRALIN yield, supported by lignin-derived reactions and gas-phase kinetics (e.g., $H + CH_4 = H_2 + CH_3$, $CH_2 + NCN = CN + H_2CN$), explains naphthyl's secondary origin and tetralin's role as a bulk precursor via dehydrogenation.

3.8. Effect of dew point temperature of PAHs species during pyrolysis

The dew point temperature of PAHs species, defined as the temperature at which these compounds in the pyrolysis vapors condense into tars, plays a critical role in the formation and distribution of PAHs in biochar. During pyrolysis, if the reactor or material temperature falls below the dew point of specific PAHs, these compounds can condense from the vapor phase onto the biochar, potentially increasing the presence of toxic PAH contaminants [96]. The dew point of PAHs is typically much higher than that of water (which is 100 °C or below at standard pressure and irrelevant in the high-temperature pyrolysis environment where water remains in the gas phase). Therefore, maintaining reactor temperatures well above the dew point of PAHs is essential to minimize their condensation and incorporation into the biochar.

When the pyrolysis temperature exceeds the dew point of PAHs, these compounds are more likely to remain in the vapor phase, reducing their deposition onto the biochar. This, in turn, influences the carbon content, surface area, and pore structure of the biochar by limiting the formation of tar-like residues. Additionally, high temperatures at the extraction point promote the release of volatile compounds, including PAHs, thereby reducing their concentration in the final char product [97]. By carefully controlling the pyrolysis temperature relative to the dew point of PAHs, the risk of toxic PAH contamination in biochar can be significantly mitigated.

Decreased reactor temperatures can result in a higher concentration of high-molecular-weight PAH species in the biochar, as they are less volatile and can be trapped in the solid matrix. As shown in Fig. 12, increasing reactor pressure to 1Mpa at 500 °C the percentage of large molecular weight PAHs species phenanthrene, anthracene, fluoranthene, pyrene and chrysene increased. According to the report [98], an increase in pressure to 1Mpa, even at a high pyrolysis temperature of 600 °C, enhances the tar component or phenol concentration. The distribution of PAH species in biochar can be influenced by the interplay between the dew point temperature, pyrolysis temperature, and feedstock properties [99,100]. The PAH dew point discussion addresses exploratory scenarios and potential process variations, thereby demonstrating design robustness. This highlights the importance of maintaining temperatures above elevated dew points in specialized high-pressure systems or during pressure fluctuations, because increased pressure raises PAH dew point temperatures, potentially affecting the condensation of larger molecular weight PAHs. Careful control of the dew point temperature during pyrolysis can help optimize the PAH profile in the resulting biochar, minimizing the presence of potentially toxic high-molecular-weight PAHs.

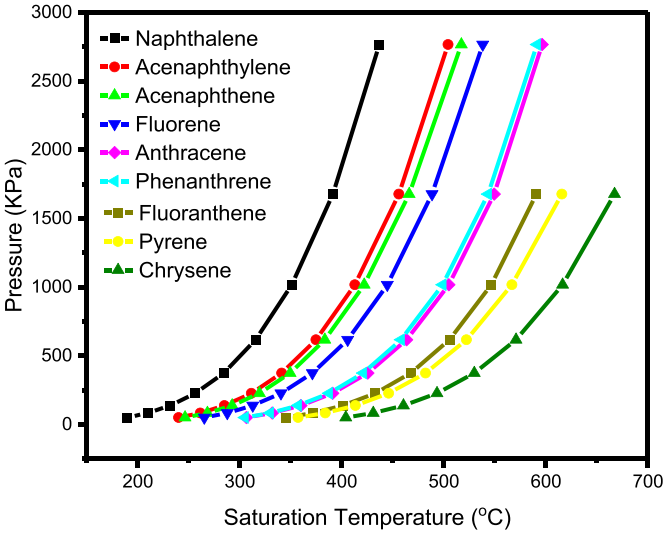

Fig. 12. Dew point curve of PAH species.

4. Conclusions

The CRECK model was used to study the interplay of pyrolysis parameters and feedstock composition on PAH formation during biomass pyrolysis. This simulation-based approach predicts PAH formation at the core stage, providing early insights into their environmental and health impacts. The detailed analysis revealed several key findings regarding the influence of individual parameters.

- **Heating Rate:** The impact of heating rate is highly temperature-dependent. At low temperatures (350 °C), higher heating rates were found to hinder PAH formation due to insufficient heat transfer to the biomass. Conversely, at 550 °C and above, increased heating rates generally promoted PAH formation. A more complex relationship was observed in the intermediate range (450–550 °C), where a heating rate of 10 °C min^{-1} often yielded the maximum fraction for most PAH species, likely due to a critical balance between enhanced volatile release and subsequent secondary gas-phase reactions.
- **Temperature:** PAH generation is particularly active within the 450–550 °C range, representing a critical balance for volatile formation and secondary reactions. While higher temperatures (above 550 °C) can lead to the decomposition of some PAHs, they concurrently facilitate the formation of larger, more stable PAH compounds.
- **Residence Time:** The residence time significantly influences PAH formation, especially at 450 °C. Generally, increasing residence time from seconds to 3000 s (50 min) promoted PAH formation. However, optimal residence times varied by PAH species; lighter PAHs like naphthalene ($C_{10}H_8$) peaked at intermediate durations, while heavier PAHs like pyrene ($C_{16}H_{10}$) reached maximum concentrations at higher temperatures (550–650 °C) and shorter residence times (6–300 s). This suggests that careful control of residence time is crucial, with durations greater than 50 min effectively balancing formation and preventing excessive cracking.
- **Feedstock Chemical Composition:** Feedstock composition plays a significant role, exhibiting complex interactions with temperature and heating rate. For instance, at 350 °C and 2 °C min^{-1}, coffee husk (with higher lignin content) produced more PAHs than corncob (with higher cellulose content). However, this trend reversed at 450 °C, with corncob yielding a higher percentage of PAHs, likely due to the higher temperature favoring cellulose decomposition and subsequent PAH precursor formation. This intricate relationship underscores the need to consider feedstock-specific responses to pyrolysis conditions.

These findings collectively demonstrate that the interaction between residence time, heating rate, and temperature significantly influences the composition and quantity of PAH species formed. Notably, this study identifies specific conditions under which PAH formation can be minimized: temperatures exceeding 500 °C, a low heating rate of 2 °C min^{-1}, and extended biomass residence times beyond 50 min. This extended duration promotes enhanced secondary reactions of pyrolytic intermediates, cracking larger PAHs and preventing their accumulation. This highlights a critical mechanistic insight: minimizing PAH formation is intrinsically linked to maximizing these secondary reactions. While maintaining bulk vapor for such prolonged periods is impractical, the model offers significant implications for process design.

The novelty of this work lies in its comprehensive application of the CRECK-S-B kinetic model, coupled with the OpenSmoke gas-phase batch reactor model, to simulate the mass fractions of USEPA-listed PAH species. This approach provides a more accurate and early-stage prediction of PAH formation, offering valuable guidance for researchers and industry practitioners aiming to produce safer and more environmentally friendly biochar. The insights gained are crucial for optimizing biochar production processes to reduce environmental risks associated with PAH contamination, contributing to the broader goals of sustainable agriculture and environmental protection.

CRediT authorship contribution statement

Teka Tesfaye Mengesha: Writing – original draft, Methodology, Formal analysis, Data curation, Conceptualization. **Venkata Ramayya Ancha:** Writing – review & editing, Supervision, Formal analysis, Conceptualization. **Alberto Cuoci:** Writing – review & editing, Visualization, Supervision. **Bruno Glaser:** Writing – review & editing, Visualization, Supervision. **Annett Pollex:** Writing – review & editing, Visualization, Supervision.

Model limitations, summary of advantages and future directions

The current model provides a quantitative prediction of the total gross formation of PAHs during the pyrolysis process. However, it is crucial to acknowledge the specific scope and boundaries of the model, which give rise to several limitations that offer clear directions for future research.

- ➢ Exclusion of PAH Phase Partitioning: The model is designed to predict the cumulative yield of PAHs generated at the core stage of pyrolysis. It does not, however, simulate the subsequent and critical redistribution of these compounds between the gas phase (pyrolysis vapors) and the solid phase (adsorption onto biochar). The complex physical phenomena of PAH recondensation, adsorption, and desorption, which are dependent on reactor conditions and biochar surface characteristics, are not incorporated into the current framework. This means the model answers the question of how much PAH is formed in total, but not where the PAH ultimately resides.
- ➢ Discrepancy Between Model Prediction and Validation Data: A significant consequence of the above limitation is a fundamental mismatch between the model's output and the experimental data used for its validation. The model predicts the total PAH yield, encompassing both volatile and condensed/adsorbed fractions. However, due to a well-documented scarcity of experimental data that quantifies PAHs in-situ or in the vapor phase under these specific pyrolysis conditions, the model validation was necessarily performed against reported literature values for PAHs adsorbed on the final biochar product. When comparing the model's output (total PAH formation) against experimental data for PAHs measured in biochar, the predictions may appear to be an overestimation. This discrepancy should not be interpreted as an inaccuracy in the prediction of PAH formation, but rather as a direct result of the validation data not accounting for the significant portion of PAHs that remained in the vapor phase and exited the reactor.

While the current model has clear limitations regarding the final distribution of PAHs, its ability to predict the total gross formation is a strategically important and valuable first step.

- ➢ Establishes a Critical Baseline and "Worst-Case" Scenario: The model quantifies the total pollutant load generated at the source. This figure represents the absolute maximum amount of PAHs that could potentially contaminate any of the pyrolysis products (biochar, bio-oil, or gas). This "worst-case" baseline is essential for comprehensive risk assessment, environmental impact studies, and designing appropriately scaled downstream cleanup technologies.
- ➢ Enables Proactive Process Optimization at the Source: The most effective way to reduce PAH contamination is to prevent its formation in the first place. By predicting the total PAH yield, the model allows researchers and engineers to understand how process parameters (like temperature, heating rate, residence time and feedstock type) influence PAH generation. This enables a proactive approach to optimize the pyrolysis process itself for inherently lower toxicity, rather than relying solely on reactive, post-process cleanup.
- ➢ Provides the Essential Foundation for More Complex Models: A complete model that includes the partitioning of PAHs between the gas and solid phases cannot be built without first knowing the total amount of PAHs being generated. The output of this formation model serves as the necessary input for a future, more sophisticated partitioning sub-model. It logically decouples the complex chemistry of formation from the complex physics of adsorption and condensation, which is a sound scientific strategy.
- ➢ Focuses on Fundamental Chemistry: By isolating the phenomenon of PAH formation, the model provides clearer insights into the core chemical reaction pathways. This fundamental understanding is crucial for developing process conditions that can interrupt these pathways and minimize PAH production at a molecular level.

Future directions

To enhance the model's predictive power and applicability, future work will be focused on addressing these limitations.

- ➢ Development of a Partitioning Sub-Model: working to develop and integrate a sub-model to simulate the dynamic partitioning of PAHs between the gas and solid phases. Planning to extend the model to incorporate mechanisms for PAH condensation, adsorption, and desorption. This will involve incorporating principles of mass transfer, thermodynamics, and surface chemistry to predict the final concentration of PAHs adsorbed onto the biochar.
- ➢ Pursuit of Comprehensive Experimental Data: To enable a more robust validation, conducting new experiments designed to simultaneously quantify PAHs in both the pyrolysis volatiles and the biochar. This will allow for a direct, multi-faceted comparison against the model's predictions for both total formation and the final distribution, leading to a more rigorously validated and comprehensive modeling tool. This can be achieved by real-time sampling and analysis of the pyrolysis vent gases to quantify PAH concentrations in the volatile stream as a function of time.
- ➢ For maintaining bulk vapor for such prolonged periods future experimental and engineering efforts should focus on optimizing reactor configurations to effectively promote these beneficial secondary reactions, even with rapid vapor venting. Strategies like staged venting, internal recirculation, catalytic beds, or multi-stage reactor systems could extend the effective reaction time for intermediates, mimicking the beneficial effects of longer residence times and enabling significant PAH reduction within practical operational constraints.

Funding

Partial financial support was received from Jimma University, Office of Research and publication and Jimma Institute of Technology, Center of Excellence.

Declaration of competing interest

The authors declare no competing interest in submitting to and publishing in this journal.

Acknowledgements

The authors are very grateful to Jimma University, Office of Research Council and Jimma Institute of Technology, Center of Excellence for providing the grant to conduct this study. They are also grateful to the CRECK Modeling Group for providing OpenSMOKE++ software and Honeywell's company for providing Honeywell UniSim Design suit.

Data availability

Data that supports the findings of this study are available in the manuscript, but additional data shall be available from the corresponding author upon request.

References

[1] Q. Zhang, D. Zhang, H. Xu, W. Lu, X. Ren, H. Cai, H. Lei, E. Huo, Y. Zhao, M. Qian, X. Lin, E.M. Villota, W. Mateo, Biochar filled high-density polyethylene composites with excellent properties : towards maximizing the utilization of agricultural wastes, Ind. Crop. Prod. 146 (2020) 112185, https://doi.org/10.1016/j.indcrop.2020.112185.

[2] Q. Zhang, J. Chen, X. Guo, H. Lei, R. Zou, E. Huo, X. Kong, W. Liu, M. Wang, Z. Ma, B. Li, Mussel-inspired polydopamine-modified biochar microsphere for reinforcing polylactic acid composite films: emphasizing the achievement of excellent thermal and mechanical properties, Int. J. Biol. Macromol. 260 (2024) 129567, https://doi.org/10.1016/j.ijbiomac.2024.129567.

[3] N. Divyangkumar, N.L. Panwar, Standardization, certification, and development of biochar based fertilizer for sustainable agriculture: an overview, Environmental Pollution and Management 1 (2024) 186–202, https://doi.org/10.1016/j.epm.2024.10.001.

[4] EBC, European Biochar Certificate - Guidelines for a Sustainable Production of Biochar, Carbon Standards International (CSI), Frick, Switzerland, 2012-2024. Version 10.4 from 20th Dec 2024), http://european-biochar.org.

[5] R. Luo, W. Schrader, Physical removal of PAXHs from highly contaminated soil by density differentiation : studying the effectiveness on the molecular level, Environmental Science Processes & Impacts 26 (1) (2024) 136–145, https://doi.org/10.1039/D3EM00379E.

[6] F. Ruggieri, A. Biancolillo, A.A. D'Archivio, F. Di Donato, M. Foschi, M.A. Maggi, C. Quattrociocchi, Quantitative structure – retention relationship analysis of polycyclic aromatic compounds in ultra-high performance chromatography, Molecules 28 (7) (2023), https://doi.org/10.3390/molecules28073218.

[7] E. Szatyłowicz, E. Hawrylik, Assessment of migration of PAHs contained in soot of solid fuel combustion into the aquatic environment, water 14 (19) (2022), https://doi.org/10.3390/w14193079.

[8] Z.-M. Wang, X. Zhang, J.-M. Lei, K.-R. Jin, Du Wang, Z.-Y. Tian, Revisit the PAH and soot formation in high-temperature pyrolysis of methane, J. Anal. Appl. Pyrolysis 182 (2024) 106668, https://doi.org/10.1016/j.jaap.2024.106668.

[9] A.G. Adeniyi, K.O. Iwuozor, E.C. Emenike, M.A. Amoloye, J.A. Adeleke, E. O. Omonayin, J.O. Bamigbola, H.T. Ojo, A.O. Ezzat, Leaf-based biochar : a review of thermochemical conversion techniques and properties, J. Anal. Appl. Pyrolysis 177 (2024) 106352, https://doi.org/10.1016/j.jaap.2024.106352.

[10] R. Muzyka, E. Misztal, J. Hrabak, S.W. Banks, M. Sajdak, Various biomass pyrolysis conditions influence the porosity and pore size distribution of biochar, Energy 263 (2023) 126128, https://doi.org/10.1016/j.energy.2022.126128.

[11] T.R. Praveenkumar, M. Sekar, R.R. Pasupuleti, B. Gavurová, G. Arun Kumar, M. Vignesh Kumar, Current technologies for plastic waste treatment for energy recovery, it's effects on poly aromatic hydrocarbons emission and recycling strategies, Fuel 357 (2024) 129379, https://doi.org/10.1016/j.fuel.2023.129379.

[12] L. Li, Z. Luo, F. Miao, L. Du, K. Wang, Prediction of product yields from lignocellulosic biomass pyrolysis based on gaussian process regression, J. Anal. Appl. Pyrolysis 177 (December 2023) (2024) 106295, https://doi.org/10.1016/j.jaap.2023.106295.

[13] Ş. Taşar, Estimation of pyrolysis liquid product yield and its hydrogen content for biomass resources by combined evaluation of pyrolysis conditions with proximate-ultimate analysis data: a machine learning application, J. Anal. Appl. Pyrolysis 165 (2022) 105546, https://doi.org/10.1016/j.jaap.2022.105546.

[14] A.K. Vuppaladadiyam, S.S. Varsha Vuppaladadiyam, V.S. Sikarwar, E. Ahmad, K. K. Pant, M. S, A. Pandey, S. Bhattacharya, A. Sarmah, S.-Y. Leu, A critical review on biomass pyrolysis: reaction mechanisms, process modeling and potential challenges, J. Energy Inst. 108 (2023) 101236, https://doi.org/10.1016/j.joei.2023.101236.

[15] H.A. Alharbi, K.D. Alotaibi, M.H. EL-Saeid, J.P. Giesy, Polycyclic aromatic hydrocarbons (PAHs) and metals in diverse biochar products: effect of feedstock type and pyrolysis temperature, Toxics 11 (2023) 96, https://doi.org/10.3390/toxics11020096.

[16] G. Lezcano, I. Hita, Y. Attada, A. Bendjeriou-sedjerari, A.H. Jawad, A. Lozano-ballesteros, M. Sun, N. Al-mana, M. Alamer, E.Z. Albaher, P. Castano, Selective ring-opening of polycyclic to monocyclic aromatics : a data- and technology-oriented critical review, Prog. Energy Combust. Sci. 99 (2023) 101110, https://doi.org/10.1016/j.pecs.2023.101110.

[17] A. Locaspi, M. Pelucchi, T. Faravelli, Towards a lumped approach for solid plastic waste gasification: polystyrene pyrolysis, J. Anal. Appl. Pyrolysis 171 (2023) 105960, https://doi.org/10.1016/j.jaap.2023.105960.

[18] S. Dong, S.W. Wagnon, L.P. Maffei, G. Kukkadapu, A. Nobili, Q. Mao, M. Pelucchi, L. Cai, K. Zhang, M. Raju, T. Chatterjee, W.J. Pitz, T. Faravelli, H. Pitsch, P. K. Senecal, H.J. Curran, A new detailed kinetic model for surrogate fuels: c3MechV3.3, Applications in Energy and Combustion Science 9 (2022) 100043, https://doi.org/10.1016/j.jaecs.2021.100043.

[19] A. Nobili, L.P. Maffei, M. Pelucchi, M. Mehl, A. Frassoldati, A. Comandini, N. Chaumeix, Experimental and kinetic modeling study of α -methylnaphthalene laminar flame speeds, Proc. Combust. Inst. 000 (2022), https://doi.org/10.1016/j.proci.2022.08.017.

[20] S. Namysl, M. Pelucchi, L. Pratali Maffei, O. Herbinet, A. Stagni, T. Faravelli, F. Battin-Leclerc, Experimental and modeling study of benzaldehyde oxidation, Combust. Flame 211 (2020) 124–132, https://doi.org/10.1016/j.combustflame.2019.09.024.

[21] A. Hamadi, W. Sun, S. Abid, N. Chaumeix, A. Comandini, An experimental and kinetic modeling study of benzene pyrolysis with C2−C3 unsaturated hydrocarbons, Combust. Flame 237 (2022) 111858, https://doi.org/10.1016/j.combustflame.2021.111858.

[22] A. Hamadi, L.C. Piton, S. Abid, N. Chaumeix, A. Comandini, Combined high-pressure experimental and kinetic modeling study of cyclopentene pyrolysis and its reactions with acetylene, in: Proceedings of the Combustion Institute, vol.000, 2022, pp. 1–10, https://doi.org/10.1016/j.proci.2022.07.023.

[23] W. Sun, A. Hamadi, S. Abid, N. Chaumeix, A. Comandini, Probing PAH formation chemical kinetics from benzene and toluene pyrolysis in a single-pulse shock tube, Proc. Combust. Inst. 000 (2020) (2020) 1–10, https://doi.org/10.1016/j.proci.2020.06.077.

[24] A.K. Stark, A.F. Ghoniem, Quantification of the influence of particle diameter on polycyclic aromatic hydrocarbon (PAH) formation in fluidized bed biomass pyrolysis, Fuel 206 (2017) 276–288, https://doi.org/10.1016/j.fuel.2017.06.020.

[25] C. Shao, H. Wang, N. Atef, Z. Wang, B. Chen, M. Almalki, Y. Zhang, C. Cao, J. Yang, S.M. Sarathy, Polycyclic aromatic hydrocarbons in pyrolysis of gasoline surrogates (n-heptane/iso-octane/toluene, Proc. Combust. Inst. 000 (2018) 1–9, https://doi.org/10.1016/j.proci.2018.06.087.

[26] W. Pejpichestakul, A. Cuoci, A. Frassoldati, M. Pelucchi, A. Parente, T. Faravelli, Buoyancy effect in sooting laminar premixed ethylene flame, Combust. Flame 205 (2019) 135–146, https://doi.org/10.1016/j.combustflame.2019.04.001.

[27] L. Pratali Maffei, M. Pelucchi, T. Faravelli, H. Pitsch, Q. Mao, A. Nobili, Polycyclic Aromatic Hydrocarbons Evolution and Interactions with Soot Particles During Fuel Surrogate Combustion: a Rate Rule-based Kinetic Model, SAE Technical Papers, 2021, https://doi.org/10.4271/2021-24-0086.

[28] A. Nobili, L. Pratali Maffei, A. Baggioli, M. Pelucchi, A. Cuoci, C. Cavallotti, T. Faravelli, On the radical behavior of large polycyclic aromatic hydrocarbons in soot formation and oxidation, Combust. Flame 235 (2022) 111692, https://doi.org/10.1016/j.combustflame.2021.111692.

[29] M.H.B.M. Hanafi, H. Nakamura, S. Hasegawa, T. Tezuka, K. Maruta, Effects of n-Butanol blends on the formation of hydrocarbons and PAHs from fuel-rich heptane combustion in a micro flow reactor with a controlled temperature profile, Combust. Sci. Technol. 193 (12) (2021) 2085–2110, https://doi.org/10.1080/00102202.2020.1729141.

[30] X. Zhao, F. Yang, Z. Li, H. Tan, Formation and emission characteristics of PAHs during pyrolysis and combustion of coal and biomass, Fuel 378 (2024) 132935, https://doi.org/10.1016/j.fuel.2024.132935.

[31] D. Bizerra, J. Nunes, C. Barros, R. Paixão, R. Marques, F.S. Neto, J. Santos, R. Melo, B. Fernandes, M. Rios, Carnauba straw as feedstock for solid biofuel production, Advances in Environmental and Engineering Research 4 (3) (2023), https://doi.org/10.21926/aeer.2303043.

[32] A.T. Kole, B.A. Zeru, E.A. Bekele, A.V. Ramayya, Design, development, and performance evaluation of husk biomass cook stove at high altitude condition, International Journal of Thermofluids 16 (November) (2022) 100242, https://doi.org/10.1016/j.ijft.2022.100242.

[33] R. Adam, A. Pollex, T. Zeng, C. Kirsten, L. Röver, F. Berger, V. Lenz, H. Werner, Systematic homogenization of heterogenous biomass batches – industrial-Scale production of solid biofuels in two case studies, Biomass Bioenergy 173 (2023), https://doi.org/10.1016/j.biombioe.2023.106808.

[34] P.E.A. Debiagi, C. Pecchi, G. Gentile, A. Frassoldati, A. Cuoci, T. Faravelli, E. Ranzi, Extractives extend the applicability of multistep kinetic scheme of biomass pyrolysis, Energy Fuels 29 (10) (2015) 6544–6555, https://doi.org/10.1021/acs.energyfuels.5b01753.

[35] G.M. Wiggins, J.E. Parks, Using chemical reactor models to predict fluidized bed pyrolysis yields of biomass feedstocks [Online]. Available: https://info.ornl.gov/sites/publications/Files/Pub170923.pdf, June. 2022.
[36] P. Debiagi, G. Gentile, A. Cuoci, A. Frassoldati, E. Ranzi, T. Faravelli, A predictive model of biochar formation and characterization, J. Anal. Appl. Pyrolysis 134 (2018) 326–335, https://doi.org/10.1016/j.jaap.2018.06.022.
[37] M. Pourhoseinian, N. Asasian-kolur, S. Sharifian, Comparative computational fluid dynamics analysis of fast pyrolysis of agricultural feedstocks across different biomass categories, Biomass Bioenergy 180 (2024) 107026, https://doi.org/10.1016/j.biombioe.2023.107026.
[38] P. Debiagi, T. Faravelli, C. Hasse, E. Ranzi, Kinetic modeling of solid, liquid and gas biofuel formation from biomass pyrolysis, in: Z. Fang, R.L.S. Jr, L. Xu (Eds.), Production of Biofuels and Chemicals with Pyrolysis, first ed., Springer, Singapore, 2020, pp. 31–76, https://doi.org/10.1007/978-981-15-2732-6_2.
[39] M.M. Afessa, P. Debiagi, A.I. Ferreiro, M.A.A. Mendes, T. Faravelli, A. V. Ramayya, Experimental and modeling investigation on pyrolysis of agricultural biomass residues: khat stem and coffee husk for bio-oil application, J. Anal. Appl. Pyrolysis 162 (2022) 105435, https://doi.org/10.1016/j.jaap.2022.105435.
[40] D.C. Makepa, C.H. Chihobo, W.R. Ruziwa, D. Musademba, Microwave-assisted pyrolysis of pine sawdust: process modelling, performance optimization and economic evaluation for bioenergy recovery, Heliyon 9 (3) (2023) e14688, https://doi.org/10.1016/j.heliyon.2023.e14688.
[41] P. Eduardo, A. Debiagi, G. Gentile, M. Pelucchi, A. Frassoldati, A. Cuoci, T. Faravelli, E. Ranzi, Detailed kinetic mechanism of gas-phase reactions of volatiles released from biomass pyrolysis, Biomass Bioenergy 93 (2016) 60–71, https://doi.org/10.1016/j.biombioe.2016.06.015.
[42] E. Ranzi, P.E.A. Debiagi, A. Frassoldati, Mathematical modeling of fast biomass pyrolysis and bio-oil formation. Note II: secondary gas-phase reactions and bio-oil formation, ACS Sustain. Chem. Eng. 5 (4) (2017) 2882–2896, https://doi.org/10.1021/acssuschemeng.6b03098.
[43] T.T. Mengesha, V.R. Ancha, L.S. Sundar, A. Pollex, Review on the influence of pyrolysis process parameters for biochar production with minimized polycyclic aromatic hydrocarbon content, J. Anal. Appl. Pyrolysis (2024) 106699, https://doi.org/10.1016/j.jaap.2024.106699.
[44] P. Devi, A.K. Saroha, Effect of pyrolysis temperature on polycyclic aromatic hydrocarbons toxicity and sorption behaviour of biochars prepared by pyrolysis of paper mill effluent treatment plant sludge, Bioresour. Technol. 192 (2015) 312–320, https://doi.org/10.1016/j.biortech.2015.05.084.
[45] H. Lyu, Y. He, J. Tang, M. Hecker, Q. Liu, P.D. Jones, G. Codling, J.P. Giesy, Effect of pyrolysis temperature on potential toxicity of biochar if applied to the environment, Environ. Pollut. 218 (2016) 1–7, https://doi.org/10.1016/j.envpol.2016.08.014.
[46] I. Adánez-Rubio, I. Fonts, P. de Blas, F. Viteri, G. Gea, M.U. Alzueta, Exploratory study of polycyclic aromatic hydrocarbons occurrence and distribution in manure pyrolysis products, J. Anal. Appl. Pyrolysis 155 (2021), https://doi.org/10.1016/j.jaap.2021.105078.
[47] E. Alladio, E. Amante, C. Bozzolino, F. Seganti, A. Salomone, M. Vincenti, B. Desharnais, Experimental and statistical protocol for the effective validation of chromatographic analytical methods, MethodsX 7 (2020) 100919, https://doi.org/10.1016/j.mex.2020.100919.
[48] A. Krzyszczak, M.P. Dybowski, R. Zarzycki, R. Kobyłecki, P. Oleszczuk, B. Czech, Long-term physical and chemical aging of biochar affected the amount and bioavailability of PAHs and their derivatives, J. Hazard Mater. 440 (2022), https://doi.org/10.1016/j.jhazmat.2022.129795.
[49] K. Crombie, O. Masek, Pyrolysis biochar systems , balance between bioenergy and carbon sequestration, GCB Bioenergy 7 (2015) 349–361, https://doi.org/10.1111/gcbb.12137.
[50] W. Buss, I. Hilber, M.C. Graham, O. Mašek, Composition of PAHs in biochar and implications for biochar production, ACS Sustain. Chem. Eng. 10 (2022) 6755–6765, https://doi.org/10.1021/acssuschemeng.2c00952.
[51] L. Maulinda, H. Husin, N.A. Rahman, C. Meurah, Results in engineering effects of temperature and times on the product distribution of bio-oils derived from Typha latifolia pyrolysis as renewable energy, Results Eng. 18 (March) (2023) 101163, https://doi.org/10.1016/j.rineng.2023.101163.
[52] N.V. Kumar, G. Sawargaonkar, C.S. Rani, R. Pasumarthi, S. Kale, Harnessing the potential of pigeonpea and maize feedstock biochar for carbon sequestration , energy generation , and environmental sustainability, Bioresources and Bioprocessing 3 (2024), https://doi.org/10.1186/s40643-023-00719-3.
[53] M. Landrat, M. Abawalo, K. Piko, Assessing the potential of teff husk for biochar production through slow pyrolysis : effect of pyrolysis temperature on biochar yield, Energies 17 (1988) (2024), https://doi.org/10.3390/en17091988.
[54] A.C.M. Vilas-Boas, L.A.C. Tarelho, H.S.M. Oliveira, F.G.C.S. Silva, D.T. Pio, M.A. A. Matos, Valorisation of residual biomass by pyrolysis: influence of process conditions on products, Sustain. Energy Fuels 8 (2023) 379–396, https://doi.org/10.1039/d3se01216f.
[55] X. Zou, P. Debiagi, M.A. Amjed, M. Zhai, T. Faravelli, Impact of high-temperature biomass pyrolysis on biochar formation and composition, J. Anal. Appl. Pyrolysis 179 (January) (2024) 106463, https://doi.org/10.1016/j.jaap.2024.106463.
[56] J. Fernández-Ferreras, T. Llano, M.K. Kochaniec, A. Coz, Slow pyrolysis of specialty coffee residues towards the circular economy in rural areas, Energies 16 (2023), https://doi.org/10.3390/en16052300.
[57] S. Sensoz, D. Angın, Pyrolysis of safflower (charthamus tinctorius L.) seed press cake: part 1. The effects of pyrolysis parameters on the product yields, Bioresour. Technol. 99 (2008) 5492–5497, https://doi.org/10.1016/j.biortech.2007.10.046.
[58] M.Y. Guida, B. Rebbah, N. Anter, A. Medaghri-Alaoui, E.M. Rakib, A. Hannioui, Biofuels and biochars production from agricultural biomass wastes by thermochemical conversion technologies: thermogravimetric analysis and pyrolysis studies, Prog. Agric. Eng. Sci. 17 (1) (2021) 15–36, https://doi.org/10.1556/446.2021.00020.
[59] M.-S. Safdari, E. Amini, D.R. Weise, T.H. Fletcher, Comparison of pyrolysis of live wildland fuels heated by radiation vs. convection, Fuel 268 (2020) 117342, https://doi.org/10.1016/j.fuel.2020.117342.
[60] S.A. El, S. Tarek, M.K. Mohamed, Thermal degradation behaviour and chemical kinetic characteristics of biomass pyrolysis using TG/DTG/DTA techniques, Biomass Conversion and Biorefinery 14 (2023) 17779–17803, https://doi.org/10.1007/s13399-023-03926-2.
[61] M.B. Pecha, J.I.M. Arbelaez, M. Garcia-Perez, F. Chejne, P.N. Ciesielski, Progress in understanding the four dominant intra-particle phenomena of lignocellulose pyrolysis: chemical reactions, heat transfer, mass transfer, and phase change, Green Chem. 21 (11) (2019) 2868–2898, https://doi.org/10.1039/C9GC00585D.
[62] B. Iglinski, W. Kujawski, U. Kiełkowska, Pyrolysis of waste biomass : technical and process achievements, and future development—A review, Energies 16 (2023), https://doi.org/10.3390/en16041829.
[63] A.C.M. Vilas-Boas, L.A.C. Tarelho, H.S.M. Oliveira, F.G.C.S. Silva, D.T. Pio, M.A. A. Matos, Valorisation of residual biomass by pyrolysis: influence of process conditions on products, Sustain. Energy Fuels 8 (2023) 379–396, https://doi.org/10.1039/d3se01216f.
[64] J. Li, Y. Shang, W. Wei, Z. Liu, Y. Qiao, S. Qin, Y. Tian, Comparative study on pyrolysis kinetics behavior and high-temperature fast pyrolysis product analysis of coastal zone and land biomasses, ACS Omega 7 (2022) 10144–10155, https://doi.org/10.1021/acsomega.1c06363.
[65] L. Li, W. Niu, H. Cong, H. Meng, Z. Niu, X. Shen, L. Cao, X. Kong, Effects of pyrolysis temperature on the release characteristics of polycyclic aromatic hydrocarbons during pyrolysis of corn stover pellet, Bioresources 18 (1) (2023) 2112–2136, https://doi.org/10.15376/biores.18.1.2112-2136.
[66] L. Zhao, Y. Zhao, H. Nan, F. Yang, H. Qiu, X. Xu, X. Cao, Suppressed formation of polycyclic aromatic hydrocarbons (PAHs) during Fe-preloaded barley straw pyrolysis, J. Hazard Mater. (2019), https://doi.org/10.1016/j.jhazmat.2019.121033.
[67] Y. Zhao, X. Li, Y. Li, H. Bao, J. Xing, Y. Zhu, J. Nan, G. Xu, Biochar acts as an emerging soil amendment and its potential ecological risks: a review, Energies 16 (2023), https://doi.org/10.3390/en16010410.
[68] Ö. Onay, H. Koca, Modelling and optimization of the pyrolysis of low- rank lignite by central composite design (CCD) method, International Journal of Coal Preparation and Utilization (2019), https://doi.org/10.1080/19392699.2019.1656201.
[69] M. Irfan, S.A. Ghalib, S. Waqas, J.A. Khan, S. Rahman, S. Nasar, F. Mursal, A. Ali, J. Ghanim, Response surface methodology for the synthesis and characterization of bio-oil extracted from biomass waste and upgradation using the rice husk ash catalyst, ACS Omega 8 (2023) 17869–17879, https://doi.org/10.1021/acsomega.3c00868.
[70] A. Mohseni-Bandpei, M. Majlesi, M. Rafiee, S. Nojavan, P. Nowrouz, H. Zolfagharpour, Polycyclic aromatic hydrocarbons (PAHs) formation during the fast pyrolysis of hazardous health-care waste, Chemosphere 227 (2019) 277–288, https://doi.org/10.1016/j.chemosphere.2019.04.028.
[71] H.R. Zolfagharpour, P. Nowrouz, A. Mohseni-bandpei, M. Majlesi, M. Rafiee, F. Khalili, Influences of temperature, waste size and residence time on the generation of polycyclic aromatic hydrocarbons during the fast pyrolysis of medical waste, Caspian Journal of Environmental Sciences 18 (1) (2020) 47–57, https://doi.org/10.22124/cjes.2020.3978.
[72] A.K. Sakhiya, A. Anand, I. Aier, V.K. Vijay, P. Kaushal, Suitability of rice straw for biochar production through slow pyrolysis: product characterization and thermodynamic analysis, Bioresour. Technol. Rep. 15 (2021) 100818, https://doi.org/10.1016/j.biteb.2021.100818.
[73] Z.A. Khan, P. Hellier, N. Ladommatos, A. Almaleki, Sampling of gas-phase intermediate pyrolytic species at various temperatures and residence times during pyrolysis of methane , ethane , and butane in a high-temperature flow reactor, Sustainability 15 (2023) 6183, https://doi.org/10.3390/su15076183.
[74] S. Xu, I. Butler, I. Go, J.A. Kozinski, Evolution of naphthalene and its intermediates during oxidation in subcritical/supercritical water, Proc. Combust. Inst. 33 (2011) 3185–3194, https://doi.org/10.1016/j.proci.2010.09.010.
[75] E.S. Odinga, F.O. Gudda, M.G. Waigi, J. Wang, Y. Gao, Occurrence , formation and environmental fate of polycyclic aromatic hydrocarbons in biochars, Fundamental Research 1 (3) (2021) 296–305, https://doi.org/10.1016/j.fmre.2021.03.003.
[76] M. Altarawneh, L. Ali, Formation of polycyclic aromatic hydrocarbons (PAHs) in thermal systems : a comprehensive mechanistic review, Energy Fuels 38 (2024) 21735–21792, https://doi.org/10.1021/acs.energyfuels.4c03513.
[77] P. Andrzej, A. Onopiuk, J. Kielar, J. Chojnacki, L. Kukiełka, J. Najser, M. Mikeska, B. Knutel, B. Berner, Polycyclic aromatic hydrocarbons (PAHs) in wheat straw pyrolysis products produced for energy purposes, Sustainability (2024) 1–14, https://doi.org/10.3390/su16229639.
[78] K. Wang, J. Remón, Z. Jiang, W. Ding, Recent advances in the preparation and application of biochar derived from lignocellulosic biomass: a mini review, Polymers 16 (2024), https://doi.org/10.3390/polym16060851.
[79] K. Klemencova, B. Grycova, P. Lestinsky, Influence of miscanthus rhizome pyrolysis operating conditions on products properties, Sustainability 14 (2022), https://doi.org/10.3390/su14106193.
[80] A. Mukherjee, B.R. Patra, J. Podder, A.K. Dalai, Synthesis of biochar from lignocellulosic biomass for diverse industrial applications and energy harvesting:

effects of pyrolysis conditions on the physicochemical properties of biochar, Frontiers in Materials 9 (2022), https://doi.org/10.3389/fmats.2022.870184.
[81] F. Amalina, A. Syukor Abd Razak, S. Krishnan, H. Sulaiman, A.W. Zularisam, M. Nasrullah, Advanced techniques in the production of biochar from lignocellulosic biomass and environmental applications, Cleaner Materials 6 (2022) 100137, https://doi.org/10.1016/j.clema.2022.100137.
[82] D. Chen, K. Cen, X. Zhuang, Z. Gan, J. Zhou, Y. Zhang, H. Zhang, Insight into biomass pyrolysis mechanism based on cellulose , hemicellulose , and lignin : evolution of volatiles and kinetics , elucidation of reaction pathways , and characterization of gas , biochar and bio-oil, Combust. Flame 242 (2022) 112142, https://doi.org/10.1016/j.combustflame.2022.112142.
[83] M. Bielecki, V. Zubkova, Analysis of interactions occurring during the pyrolysis of lignocellulosic biomass, Molecules 28 (2023), https://doi.org/10.3390/molecules28020506.
[84] L. Martínková, M. Grulich, M. Pátek, B. Krístková, M. Winkler, Bio-based valorization of lignin-derived phenolic compounds : a review, Biomolecules 13 (2023) 717, https://doi.org/10.3390/biom13050717.
[85] Y. Ma, J. Lin, M. Li, Y. Zhu, L. Zhao, D. Liang, D.H. Cho, G. Zhao, Effect of lignin on the formation of polycyclic aromatic hydrocarbons in smoked and grilled meat products, Int. J. Biol. Macromol. 261 (2024) 129574, https://doi.org/10.1016/j.ijbiomac.2024.129574.
[86] P. Nargotra, V. Sharma, M.-L. Tsai, S.-L. Hsieh, C.-D. Dong, H.-M.D. Wang, C.-H. Kuo, Recent advancements in the valorization of agro-industrial food waste for the production of nanocellulose, Appl. Sci. 13 (2023), https://doi.org/10.3390/app13106159.
[87] T.E. Mcgrath, W.G. Chan, R. Hajaligol, Low temperature mechanism for the formation of polycyclic aromatic hydrocarbons from the pyrolysis of cellulose, J. Anal. Appl. Pyrolysis 66 (2003) 51–70.
[88] H. Zhang, X. Zhang, Y. Wang, P. Bai, K. Hayakawa, L. Zhang, N. Tang, Characteristics and influencing factors of polycyclic aromatic hydrocarbons emitted from open burning and stove burning of biomass: a brief review, Environmental Research and Public Health 19 (2022), https://doi.org/10.3390/ijerph19073944.
[89] W. Li, N. Wanninayake, X. Gao, M. Li, Y. Pu, D.-Y. Kim, A.J. Ragauskas, J. Shi, Mechanistic insight into lignin slow pyrolysis by linking pyrolysis chemistry and carbon material properties, ACS Sustain. Chem. Eng. 8 (2020) 15843–15854, https://doi.org/10.1021/acssuschemeng.0c03423.
[90] M.C. Mosonik, R. Volpe, C. Ezenwajiaku, M. Talibi, R. Balachandran, In situ observation of the evolution of polyaromatic tar precursors in packed-bed biomass pyrolysis, React. Chem. Eng. 6 (2021), https://doi.org/10.1039/d1re00032b.
[91] Y. Liu, Y. Liu, R. Chen, H. Wang, H. Gao, Y. Wang, J. Wang, Microwave pyrolysis of sewage sludge for bio-oil production : effects of organic components and mechanisms, Fuel Process. Technol. 253 (2024) 108023, https://doi.org/10.1016/j.fuproc.2023.108023.
[92] S. Erlend, K.M. Krahn, Ø. Gudny, T. Hartnik, H. Peter, H. Arp, G. Cornelissen, Distribution of PAHs , PCBs , and PCDD/Fs in products from full-scale relevant pyrolysis of diverse contaminated organic waste, Hazardous Materials 461 (2024), https://doi.org/10.1016/j.jhazmat.2023.132546.
[93] H.A. Alharbi, K.D. Alotaibi, M.H. EL-Saeid, J.P. Giesy, Polycyclic aromatic hydrocarbons (PAHs) and metals in diverse biochar products: effect of feedstock type and pyrolysis temperature, Toxics 11 (2023), https://doi.org/10.3390/toxics11020096.
[94] T.-C. Chu, M.C. Smith, J. Yang, M. Liu, W.H. Green, Theoretical study on the HACA chemistry of naphthalenyl radicals and acetylene: the formation of C12H8, C14H8, and C14H10 species, Chemical Kinetics 52 (11) (2020) 1–27, https://doi.org/10.1002/kin.21397.
[95] R. Langer, Q. Mao, H. Pitsch, A detailed kinetic model for aromatics formation from small hydrocarbon and gasoline surrogate fuel combustion, Combust. Flame 258 (2023) 112574, https://doi.org/10.1016/j.combustflame.2022.112574.
[96] W. Buss, M.C. Graham, G. MacKinnon, O. Mašek, Strategies for producing biochars with minimum PAH contamination, J. Anal. Appl. Pyrolysis 119 (2016) 24–30, https://doi.org/10.1016/j.jaap.2016.04.001.
[97] D. Ronga, E. Francia, G. Allesina, S. Pedrazzi, M. Zaccardelli, C. Pane, A. Tava, C. Bignami, Valorization of vineyard By-Products to obtain composted digestate and biochar suitable for nursery grapevine (Vitis vinifera L) production, Agronomy 420 (2019), https://doi.org/10.3390/agronomy9080420.
[98] F. Wang, N. Gao, A. Magdziarz, C. Quan, Co-Pyrolysis of biomass and waste tires under high-pressure two-stage fixed-bed reactor, Bioresour. Technol. 344 (2022), https://doi.org/10.2139/ssrn.3929266.
[99] S. Papari, K. Hawboldt, A Review on Condensing System for Biomass Pyrolysis Process, vol. 180, 2018, pp. 1–13, https://doi.org/10.1016/j.fuproc.2018.08.001.
[100] A. Mati, M. Buffi, S.D. Orco, G. Lombardi, P. Maria, R. Ramiro, S.R.A. Kersten, D. Chiaramonti, Applied sciences fractional condensation of fast pyrolysis bio-oil to improve biocrude quality towards alternative fuels production, Applied Research 12 (2022), https://doi.org/10.3390/app12104822.